R. & M. No. 3715

R. & M. No. 3715


MINISTRY OF DEFENCE (PROCUREMENT EXECUTIVE)

AERONAUTICAL RESEARCH COUNCIL
REPORTS AND MEMORANDA

# An Experimental Investigation of Wind-Tunnel Wall Conditions for Interference-Free Dynamic Measurements

By A. W. MOORE and K. C. WIGHT
Aerodynamics Division, NPL

LONDON: HER MAJESTY'S STATIONERY OFFICE
1973

PRICE £1·70 NET

# An Experimental Investigation of Wind-Tunnel Wall Conditions for Interference-Free Dynamic Measurements

By A. W. MOORE and K. C. WIGHT

Aerodynamics Division, NPL

*Reports and Memoranda No.* 3715*
*December*, 1969

SUMMARY

Results are presented of dynamic tests on two model half-wings performing pitching oscillations in the NPL 24 cm × 24 cm (9½ in × 9½ in) tunnel. The boundary condition at the ventilated roof and floor is varied by fitting perforated channels behind the longitudinal slots such that the size of the perforations can be varied from zero to 0·79 cm (0·31 in) diameter circular holes. It is found that the measured derivatives each vary systematically with changing porosity and a method is suggested for selecting a wall porosity to give interference-free damping derivatives; interference-free stiffness derivatives are not simultaneously obtained and small corrections to measured values are required.

A porosity parameter for the ventilated wall is defined, values of this parameter are measured and consideration is given to the value required to minimize wall interference in the NPL tunnel and other tunnels of different shape or different slot configuration.

* Replaces NPL Aero Report 1307—A.R.C. 31 704.

LIST OF CONTENTS

## 1. Introduction

Previous investigations of wall constraint on dynamic measurements in ventilated wind tunnels have provided a fundamental understanding of the large effects on damping derivatives[1,2], but no practical method for reducing the interference has been established. From a theoretical study of interference at subsonic speeds[1], it was concluded that a tunnel having ventilated side-walls with a solid roof and floor would give acceptably small ventilated-wall effects, but at transonic and low supersonic speeds one might expect wave reflection from the solid walls which would impose severe limitations on the size of model. Furthermore, many existing transonic tunnels have ventilations only in the roof and floor, and the cost of modifications necessary to achieve a satisfactory working section of the type suggested could be prohibitive. It is therefore desirable to investigate the effects of alterations in the characteristics of the ventilated walls, with the aim of minimizing any large interference effects in existing transonic tunnels by a simple modification to the tunnel walls.

In Ref. 1 it is noted that in one NPL slotted tunnel, which has a thick boundary layer compared with slot width, there is little difference at subsonic speeds, $M < 0{\cdot}8$, between damping measured with slots open and damping measured with slots sealed, although a significantly large change is expected theoretically. Another tunnel, with an identical slotted wall but with a thinner boundary layer, gives an intermediate result in that the changes in damping obtained on sealing the slots are about 70 per cent of the changes predicted theoretically. These differences between theory and experiment are thought to be caused by the influence of the boundary layer which makes each slotted wall behave more like a sealed wall than an ideal slotted boundary. A linearized equation describing viscous effects at a slotted wall in steady flow introduces a porosity parameter relating the mass flow through the wall to the pressure drop across the wall. Since ventilated-wall interference with no boundary-layer effects generally has the opposite sign to interference with ventilations sealed, it seems likely that a suitable choice of porosity at the slotted wall might give interference-free measurements. It happens that the linearized boundary condition for the inviscid steady flow at a perforated wall involves a porosity parameter of similar form to that describing viscous effects at a slotted wall; so the present report considers the effects of varying the porosity of the slotted-perforated wall described in Section 2. This is basically a slotted wall which has very wide slots compared with boundary-layer displacement thickness, but behind each slot is fitted a perforated channel whose perforations can be varied in size. Results of calibration tests given in Section 4 show that transonic speeds can be achieved satisfactorily in the modified tunnel and that the porosity parameter for the wall is almost independent of Mach number when $M > 0{\cdot}6$. In Section 5, it is seen that with the fairly low frequency of oscillation used ($\bar{\nu} < 0{\cdot}15$), the derivatives obtained with varying porosity all change systematically from values appropriate to a sealed tunnel to values appropriate to a slotted tunnel as porosity is varied from zero to infinity. Measurements made with two half-wings of different planform show that a suitable choice of porosity for the modified tunnel walls virtually eliminates the interference on damping derivatives for both wings over the whole range of Mach number of the tests, i.e., $0{\cdot}4 \leqslant M \leqslant 1{\cdot}05$. This suggests a promising practical method for reducing the large wall interference effects on dynamic measurements.

## 2. Apparatus

All the measurements were made in the NPL 24 cm × 24 cm ($9\frac{1}{2}$ in × $9\frac{1}{2}$ in) slotted tunnel with the oscillating rig and analysing equipment previously used in the investigation of Ref. 1. The bulk of the work was done with a half-wing of cropped-delta planform but some results were obtained with a half-wing of unswept tapered planform similar to a larger model used in earlier tests[1]; planforms and details of the models are shown in Fig. 1. Boundary-layer transition was fixed near the leading edge of each model by a carborundum roughness strip. The tunnel has streamwise slots in the roof and floor, and for the present investigation the usual walls with 16 slots were replaced by modified slotted walls each having five slots 0·76 cm (0·30 in) wide to give the same open area ratio of 15 per cent as the previous walls. Since the tunnel boundary layer displacement-thickness at the cross-section containing the half-model is only about 0·28 cm (0·11 in) the new walls with no attachments have negligible viscous effects in the slots. These 'ideal' slotted walls give a reduced interference effect on dynamic measurements compared

with the previous walls because there is now a significantly large slot parameter. Nevertheless, changes in damping of about 100 per cent are obtained on sealing the slots.

The configuration adopted to obtain variable porosity at the slotted walls is shown schematically in Fig. 2. Behind each slot is fitted a 2·5 cm × 1·6 cm (1·0 in wide × 0·6 in deep) aluminium channel which has circular holes 0·79 cm (0·31 in) in diameter drilled in its base in a staggered pattern. A wooden runner slides in the base of the channel, and this is perforated with an identical pattern of circular holes such that the nett perforation size obtained can be changed from one extreme of circular holes to another extreme of an effective closed wall. The runners are moved independently by levers at the end of the tunnel wall and, to set an intermediate perforation size for a given channel, the lever is adjusted until the wooden runner comes firmly against a rod of chosen diameter inserted through the wall; the lever arm is then locked in position and the operation repeated for each of the other channels. This method was adopted as a convenient simple means for varying wall porosity, but it might be noted that since perforation size and open area ratio were simultaneously changed, it was not possible to determine their individual effects on the wall boundary condition.

## 3. Measurements

Pitching-moment derivatives were measured with five perforation sizes chosen so that the wall porosity could be varied progressively from zero (closed tunnel) to infinity (perforations removed). For all values except zero porosity when the maximum Mach number was about 0·85, tests were made at speeds $0{\cdot}4 \leqslant M \leqslant 1{\cdot}05$. The axes of oscillation for the half-delta wing were at $x_0 = 0{\cdot}31\,\bar{c}$, $x_0 = 0{\cdot}65\,\bar{c}$ and $x_0 = 1{\cdot}04\,\bar{c}$, but only two axis positions were used in tests on the unswept tapered wing namely, $x_0 = 0{\cdot}395\,\bar{c}$ and $x_0 = 1{\cdot}185\,\bar{c}$. Most of the measurements were made with a nominal frequency of oscillation of 53 Hz although there were a few additional tests on the half-delta wing at frequencies 19 Hz and 87 Hz. Only pitching-moment derivatives could be measured with the decaying oscillation technique used; so lift derivatives were calculated from the axis transfer equations (Section 5).

## 4. Porosity of the Ventilated Walls

The changes in tunnel interference obtained by varying the perforations in the channels fitted behind the slots can be discussed without any reference to wall porosity. Indeed, given an interference-free datum, a perforation size can be found which gives negligible interference effects on oscillatory derivatives measured in the 24 cm × 24 cm ($9\frac{1}{2}$ in × $9\frac{1}{2}$ in) tunnel. But this has limited general application because only the method for reducing wall interference is verified with no indication of the fundamental reason for the changes involved. Furthermore, for comparison with the results of any future theoretical attack on the problem, a knowledge of the basic changes in boundary condition caused by varying the perforations must be available. Hence, in the Appendix there is a discussion of definitions of a boundary condition for ventilated walls and an equation is given which defines the boundary condition appropriate to a slotted-perforated wall in terms of a porosity parameter $P_E$. The equation is

$$\frac{\Delta p}{q_\infty} = \frac{2}{P_E}\frac{\rho v_n}{\rho_\infty U_\infty} \tag{1}$$

which relates the pressure drop across the wall ($\Delta p$) to the mass flow per unit area through the wall ($\rho v_n$). $U_\infty$, $\rho_\infty$ and $q_\infty$ are the speed, density and dynamic pressure of the undisturbed tunnel flow.

To calibrate the wall at a given Mach number, the ends of the plenum chamber are sealed and auxiliary suction is used to draw air through a 55 cm × 8·9 cm (21·7 in × 3·5 in) slot in the outer wall. The mass of air drawn through the wall is measured with a venturi meter, and the corresponding pressure drop across the wall is determined from pressures measured at tappings distributed along the centre-line of the tunnel and from pressures measured at the six positions in the plenum chamber shown in Fig. 3.

Typical results for a range of perforation size with M = 0·8 are shown in Fig. 4. It is evident that although predominantly linear relationships between mass outflow and pressure drop are obtained, the lines shown will not pass through the origin as would be expected from equation (1). This effect will not pass the origin as would be expected from equation (1). This effect has been noted before (e.g., in Fig. 11, 17a of

Ref. 3) and if measurements could be obtained down towards zero outflow, the near-linear trend would abruptly cease with mass outflow tending to zero at a low positive value of the pressure ratio $\delta p/q_\infty$. The non-linearity arises because initially the applied suction only thins the boundary layer on the perforated wall; the linear characteristics of an ideal perforated wall will not be obtained until the boundary layer is removed or sufficiently thinned. When derivative measurements were made with the normal operating conditions of the tunnel, tests confirmed that the pressure drop across the ventilated wall was large enough to lie in the linear range of the calibration measurements. The pressure drop obtained with the 0·16 cm (0·06 in) perforations was only marginally in the linear range and it was decided that this was the smallest non-zero perforation size which would be used. With perforations shut, leakage around the edges of the perforated channel and through the end of the plenum chamber means that a flow through the plenum chamber is obtained when suction is applied. A strongly non-linear plot of leakage mass flow against pressure drop is obtained and this had been subtracted from the total flow through the wall with open perforations as given in Fig. 4 on the assumption that the leakage rate is constant for a given pressure drop across the wall. Only the results for the 0·16 cm (0·06 in) perforations are appreciably changed by this correction since the mass flow due to leakage is usually very small compared with the mass flow with perforations open. The corrected calibration curves are similar for all speeds as can be seen indirectly from the cross plots of parameter $P_E$ against Mach number in Fig. 5a. In other words, the combined slotted-perforated wall under test gives a linear relationship between mass flow through the wall and pressure drop across the wall throughout the operating speed range. Since $P_E$ varies from zero for a closed wall to infinity for an open wall, it is convenient to use a parameter of the form $\Psi = (1 + 1/P_E)^{-1}$ which varies from zero to unity. The plots of $\Psi$ against $M$ in Fig. 5b show little variation with Mach number for $M > 0{\cdot}6$. This implies that the wall has an effectively constant porosity parameter over most of the speed range of the tests.

## 5. Discussion of Results

The values of pitching-moment derivatives $m_\theta$, $m_{\dot\theta}$ were measured with more than one position of the pitching axis and the corresponding lift derivatives $l_\theta$, $l_{\dot\theta}$ were determined from the following relations

$$l_{\theta 1} = l_{\theta 2} = \frac{m_{\theta 2} - m_{\theta 1}}{(x_2 - x_1)/\bar{c}} \tag{2}$$

and

$$l_{\dot\theta 1} - m_{\theta 2} = \frac{m_{\dot\theta 2} - m_{\dot\theta 1}}{(x_2 - x_1)/\bar{c}} = l_{\dot\theta 2} - m_{\theta 1}. \tag{3}$$

These equations are derived from the axis-transfer relations on the assumption that, for low frequency parameters,

$$\left.\begin{aligned} l_z &= m_z = 0, \\ l_{\dot z} &= l_\theta \end{aligned}\right\} \tag{4}$$

and

$$m_{\dot z} = m_\theta,$$

the subscripts 1, 2 refer to pitching axes at distances $x_1$, $x_2$ downstream of the root leading edge, $\bar{c}$ being the geometric mean chord of the model. The variation of all four derivatives with Mach number for the half-delta wing with two axis positions and various perforation sizes are shown in Figs. 6a–6d and 7a–7c. It is clear that the derivatives change consistently with perforation size throughout the speed range of the tests since curves with similar trends are obtained for different wall settings. Cross plots against porosity parameter $\Psi$ confirm that at all speeds the derivatives vary systematically with changing porosity from values with perforations shut (slots sealed), to values with perforated channels removed (slots open). Assuming that the interference-free curve lies between and has the same trend as the curves obtained with slots open and with slots sealed, it follows that a suitably chosen porosity of the slotted wall will give, say, interference-free pitching damping at all speeds. It should be emphasized that

interference-free pitching damping at all speeds. It should be emphasized that interference-free conditions can be achieved at transonic speeds even though it was demonstrated in Ref. 2 that maximum interference effects on damping can occur in this important speed range.

An interference-free datum has been measured for the present half-model but, in general, derivative values free of wall constraint will not be known *a priori*. From past experience we have confidence in applying corrections to measured derivatives for the rearward axis in the closed 24 cm × 24 cm ($9\frac{1}{2}$ in × $9\frac{1}{2}$ in) tunnel as given by the subsonic wall-interference theory of Ref. 1. Hence, a first step in achieving an interference-free ventilated wall is to calculate interference-free derivatives at subsonic speeds by correcting the derivatives with sealed walls. This calculation, based on equations (58) of Ref. 1, has been written as an ALGOL programme and the corrected points (+) are shown on Figs. 6a–6d. (It is shown later that these calculated interference-free derivatives are in good agreement with the measured interference-free values for the half-delta wing.) For the damping derivatives $m_{\dot{\theta}}$ and $l_{\dot{\theta}}$, it can be seen that the interference-free points lie very close to the results measured with 0·16 cm (0·06 in) perforations and this condition is suggested to give the required interference-free wall for damping derivatives with the model used. Unfortunately, a different wall condition is required for interference-free stiffness derivatives since these lie closest to the results measured with 0·79 cm (0·31 in) perforations. In many cases, ventilated wall effects on $l_\theta$ and $m_\theta$ are small compared with effects on damping so that errors in stiffness derivatives measured in a ventilated tunnel designed primarily to give correct damping derivatives will often be small, but in the present case there are significant changes in $l_\theta$ and $m_\theta$ on sealing the slots. A further change in perforation size would give the required interference-free values but this would mean repeating tests with two wall conditions in order to obtain both stiffness and damping derivatives. It would seem better to design for interference-free damping and apply the necessary small corrections to the measured stiffness derivatives. Such corrections can easily be estimated because the lift interference on stiffness is related predominantly to a tunnel upwash parameter ($\delta_0$) for steady flow[1], and the variation of $\delta_0$ with changing porosity for subsonic speeds can be estimated.

From tests on the half-delta wing in four NPL transonic tunnels discussed in Ref. 2, it was concluded that ventilated-wall effects at subsonic speeds persist throughout the transonic speed range. Three of the tunnels were relatively large compared with model size and gave little wall interference, whilst the 24 cm × 24 cm ($9\frac{1}{2}$ in × $9\frac{1}{2}$ in) tunnel produced considerable changes on sealing the slots. The results from the three other tunnels did not fall on a single curve because the relatively-large side-wall boundary layers caused their own interference effects. The tests have recently been repeated with the side-wall boundary layers thinned by vortex generators and satisfactory interference-free values of derivatives have been obtained[4]. These are reproduced in Figs. 8 and 9 which clearly show the severe slotted wall interference on damping derivatives measured in the 24 cm × 24 cm ($9\frac{1}{2}$ in × $9\frac{1}{2}$ in) slotted tunnel. It can be seen in Figs. 8a–8d that there are only small differences between the calculated interference-free curve, i.e., the 'corrected sealed' results and the measured interference-free datum on each figure. The damping derivatives from the present tests with 0·16 cm (0·06 in) perforations behind the slotted walls (the suggested interference-free walls) are also shown in Figs. 8a, b and 9a, b and these lie close to the interference-free curves at all speeds and for both axis positions. Some additional tests were made with the centre axis because previous measurements of pitching damping with this axis[2] showed surprising trends in the transonic speed range. Interference on $m_{\dot{\theta}}$ is approximately proportional to $m_\theta$ which for the centre axis at subsonic speeds is nearly zero because the axis passes very close to the aerodynamic centre of the half-model. As seen in Fig. 10 little interference is measured at subsonic speeds but for $M > 0{\cdot}95$ the results suddenly depart from the interference-free values. At the same time, $m_\theta$ goes negative indicating a downstream movement of the centre of pressure. It was stated with some reservation in Ref. 2 that the large difference in pitching damping is due to wall interference associated with a fairly small rearward displacement of the centre of pressure from the central axis position. From Fig. 10 it is apparent that with the 0·16 cm (0·06 in) perforations fitted the large difference between the interference-free datum and the measured pitching damping is to a great extent suppressed. This lends support to the idea that the change is due to wall interference, and also indicates that the present modified walls are giving near interference-free results on damping for all axis positions. For $M < 0{\cdot}9$ stiffness derivatives from the present tests with 0·16 cm (0·06 in) perforations behind the slotted walls do not lie close to the interference-

free curves in Figs. 8c, d and 9c. However, the results with the 0·79 cm (0·31 in) perforations agree quite well with the interference-free values, which again shows that different wall conditions are required for interference-free stiffness and interference-free damping derivatives.

With ventilated walls suitably modified to give damping derivatives free from wall constraint on one model, it is desirable to know if dynamic tests on other models of similar size are likewise free from wall interference. Pitching-moment derivatives for the unswept tapered half-wing shown in Fig. 1 have therefore been measured with slots open, with slots sealed and with 0·16 cm (0·06 in) and 0·79 cm (0·31 in) perforations behind the slotted walls. The results in Figs. 11a to 12b show that the 0·16 cm (0·06 in) perforations give only small interference on damping, although more open walls would be needed to eliminate interference since the results are closer to the values measured with slots sealed than they are to the corrected sealed-tunnel values. The corrected results for the two perforated wall conditions shown in the figures are discussed later. Results in Figs. 13 to 14 likewise show that 0·79 cm (0·31 in) perforations are required to give interference-free values of stiffness derivatives. Hence, the tests with the unswept tapered wing indicate that when the tunnel walls have been modified to give interference-free derivatives for the cropped-delta wing, then interference is reduced to small proportions in dynamic measurements on another wing having a quite different planform which suffers severe interference on damping measured in a conventional slotted tunnel.

Most of the present tests on the half-delta wing were done with a frequency of oscillation of 53 Hz. An attempt was made to investigate frequency effects on interference in the slotted-perforated tunnel by varying the frequency of oscillation from 19 Hz to 87 Hz, but the results were inconclusive. A less turbulent tunnel flow or a wider range of frequency than could be obtained with the present apparatus would be necessary in order to draw a satisfactory conclusion.

Another wind tunnel in which ventilated-wall interference has been investigated is the Hawker Siddeley Dynamics 56 cm × 51 cm (22 in × 20 in) transonic tunnel, which had gauzes fitted behind the slots in order to improve the Mach number distribution along the working section. With no gauzes, ventilated-wall interference caused large differences between results of dynamic tests on a half-model with slots open and with slots sealed. Unpublished work showed that the introduction of the gauzes had a marked effect on the damping derivatives $m_{\dot{\theta}}$, $l_{\dot{\theta}}$ so that the values with the modified walls were not far removed from the values in the closed tunnel—a probable near interference-free condition on damping for half-model tests in a square tunnel. Furthermore, in an investigation of ventilated-wall interference in the Hawker Siddeley Dynamics 25 cm × 20 cm (10 in × 8 in) slotted tunnel[5], measurements were made of the upwash ahead of an oscillating model with slots open, slots sealed and, in view of their experience with the larger tunnel, with gauzes fitted behind the slots. No measurements of porosity parameter were made, but the perforations in the gauzes were 0·28 cm (0·11 in) diameter circular holes which differ in area by only 10 per cent from the area of the present 0·16 cm (0·06 in) perforations, although the number of perforations per unit area in the Hawker Siddeley gauzes was three times that of the present wall. The slot widths and tunnel shapes were sensibly the same in both cases, so the choice of screens made for reasons other than minimizing unsteady interference gave a situation remarkably similar to the present interference-free condition for damping in the NPL 24 cm × 24 cm ($9\frac{1}{2}$ in × $9\frac{1}{2}$ in) tunnel. It is interesting to note that when the gauzes were fitted the amplitude of oscillatory upwash was significantly changed from that with open slots and lay quite close to the value with slots sealed. An oscillating upwash ahead of the model was also observed with slots open at a low supersonic speed M = 1·14. This must be solely interference upwash and when gauzes were fitted its magnitude was drastically reduced.

## 6. Modified Walls to Minimize Interference

### 6.1. Method

The suggested method for obtaining interference-free walls may be summarized as follows:

(a) Choose a model wing which has a planform amenable to theoretical treatment and which is sensitive to wall interference, e.g., a wing of fairly high aspect ratio.

(b) If the ventilations are longitudinal slots, measure pitching-moment derivatives (preferably with a

pitching axis to the rear of the centre of pressure) at some convenient subsonic Mach number, e.g., M = 0·8, with slots sealed.

(c) Correct the derivatives for sealed-wall interference using the theory of Ref. 1 (including the allowance for finite model span outlined in Section 4.2 of Ref. 1).

(d) Find, by trial, suitable perforated screens which, when fitted behind the slotted walls, give the corrected value of the pitching damping derivative $m_{\dot{\theta}}$. This configuration will then be taken to give minimal interference on damping for all axis positions and speeds, but small corrections will probably be required to the measured stiffness derivatives, in which case the steady upwash parameter $\delta_0$ appropriate to the modified walls must be calculated from the measured and corrected stiffness derivatives (Section 6.3). We assume that the working-section configuration thus established is suitable for testing any other model of similar size to the chosen wing.

(e) If the ventilated walls consist of perforations, the same procedure holds in principle but, according to Goethert[5], the porosity parameter may then vary with Mach number. This can be checked by making the initial measurements with sealed walls at several Mach numbers, one as high as is sensible, say M = 0·85. If the modified perforated walls do not give the desired damping at all speeds, either adopt the configuration chosen on the basis of the results at M = 0·85 to minimize any interference effects present at transonic speeds, or seal the perforated wall in longitudinal strips. This effectively produces a slotted wall with perforations covering the slots and was done in some dynamic tests at subsonic speeds on an unswept tapered wing pitching in the NPL 64 cm × 51 cm (25 in × 20 in) perforated tunnel[2]. The results are reproduced in Fig. 15 where the curves indicate that the effect of the combined wall is practically independent of Mach number.

### 6.2. General Notes

The method outlined for a slotted tunnel has been used in the present investigation to obtain interference-free slotted-perforated walls, and the corresponding value of porosity parameter $P_E$ has also been determined. This will not be a universal value (i.e., it will not be the same for all tunnels) because it can be shown theoretically that the lift interference on oscillatory measurements depends primarily on three parameters $\delta_0$, $\delta_1$ and $\delta'_0$ where

$\delta_0$ represents the tunnel-induced upwash at the model in steady flow,

$\delta_1$ represents the tunnel-induced streamline curvature at the model in steady flow,

$\delta'_0$ represents the in-quadrature induced upwash at the model.

Interference on damping is roughly proportional to $\delta'_0$, but all three vary with porosity parameter $P_E$, slot parameter $F$ and tunnel cross-sectional shape. Hence if slot parameter and/or tunnel shape are changed, a new value of porosity parameter $P_E$ is required for interference-free walls. It might be noted that in the present tests the effective ratio of tunnel breadth to tunnel height is large (2·6) and a low porosity is needed to give interference-free damping: for a less broad tunnel with the same slot parameter, the necessary porosity condition for interference-free damping would be obtained with a higher porosity, i.e., with the perforated channels less closed. From a practical point of view a prior knowledge of the parameter $P_E$ required for interference-free walls would be a great saving. Some idea of the trend of changes in parameter $P_E$ with changing tunnel shape and slot parameter might come from a theoretical attack on the problem. Even if reasonable theoretical trends are obtained, however, one still has the practical problem of obtaining a perforated screen which has the calculated porosity. So many factors influence the porosity of a wall that the only satisfactory way to determine $P_E$ will probably always be to calibrate samples of available perforated material. In some cases, it may be simplest to adjust a wall of variable porosity as in the present tests.

### 6.3. Residual interference

If the porosity is not adjustable, then, as shown in Section 5, once the ventilated walls have been modified to minimize interference on a particular model, wall interference will probably remain small in tests on any other model of similar size. However, since there may be some interference effects present in dynamic

tests on different models it would be of use to have a simple method for estimating the magnitude of the small errors involved. The theoretical boundary condition which represents a slotted-perforated wall includes both a slot parameter and a porosity parameter. For cases where the porosity is either zero or infinite, equations (58) of Ref. 1 relate the interference-free values of derivatives to the values measured in a tunnel as follows:

$$
\left.
\begin{aligned}
l_\theta\left\{1+\frac{2S}{C}\delta_0(l_\theta)_T+\frac{2S}{C}\frac{\delta_1\bar{c}}{\beta h}(m_\theta)_T\right\} &= (l_\theta)_T\left\{1-\frac{2S}{C}\frac{\delta_1\bar{c}}{\beta h}l_q\right\},\\
m_\theta\left\{1+\frac{2S}{C}\delta_0(l_\theta)_T+\frac{2S}{C}\frac{\delta_1\bar{c}}{\beta h}(m_\theta)_T\right\} &= (m_\theta)_T-(l_\theta)_T\frac{2S}{C}\frac{\delta_1\bar{c}}{\beta h}m_q,\\
l_{\dot\theta}\left\{1+\frac{2S}{C}\delta_0(l_\theta)_T\right\} &= (l_{\dot\theta})_T\left\{1-\frac{2S}{C}\delta_0 l_\theta-\frac{2S}{C}\frac{\delta_1\bar{c}}{\beta h}l_q\right\}-(m_{\dot\theta})_T\frac{2S}{C}\frac{\delta_1\bar{c}}{\beta h}l_\theta\\
&\quad-(l_\theta)_T\frac{2S}{C}\left\{\frac{\delta_0' h}{\beta\bar{c}}l_\theta-2\delta_0 l_q\right\}+(m_\theta)_T\frac{2S}{C}\delta_0 l_\theta\\
m_{\dot\theta}\left\{1+\frac{2S}{C}\delta_0(l_\theta)_T\right\} &= -(l_{\dot\theta})_T\frac{2S}{C}\left\{\delta_0 m_\theta+\frac{\delta_1\bar{c}}{\beta h}m_q\right\}+(m_{\dot\theta})_T\left\{1-\frac{2S}{C}\frac{\delta_1\bar{c}}{\beta h}m_\theta\right\}\\
&\quad-(l_\theta)_T\frac{2S}{C}\left\{\frac{\delta_0' h}{\beta\bar{c}}m_\theta-2\delta_0 m_q\right\}+(m_\theta)_T\frac{2S}{C}\delta_0 m_\theta,
\end{aligned}
\right\}
\tag{5}
$$

and

where suffix $T$ denotes measured values, and $l_q$ and $m_q$ are derivatives defined in equations (47) of Ref. 1 for steady rotary pitching motion.

With finite kon-zero porosity a different formulation with additional upwash parameters is necessary, but it is possible that the lift interference due to the chosen slotted-perforated walls may be the same as that given by equations (5) with empirical values of $\delta_0, \delta_1, \delta_0'$. If this is so, values of the derivatives measured on a particular planform in the tunnel with slotted-perforated walls and the corresponding calculated interference-free values can be substituted into equations (5), to give equivalent upwash interference parameters $\delta_0$, $\delta_1$, $\delta_0'$ for the chosen ventilated-wall condition. These parameters can then be used to estimate corrections to derivatives measured when other planforms are tested in the tunnel with the chosen walls.

The use of 'equivalent interference parameters' can be checked from the present measurements with two models having different planforms but equal span. First, derivatives measured in the tests on the half-delta wing in the tunnel with ventilations sealed are corrected for wall interference. Next, derivatives measured with perforations open are substituted into equations (5) together with the corresponding interference-free values, to determine the interference upwash parameters $\delta_0$, $\delta_1$, $\delta_0'$ for the chosen perforated wall.† The procedure is repeated for results at three speeds M = 0·4, 0·6, 0·8 and mean values obtained as tabulated below. The table shows that interference-free conditions for the given tunnel are achieved with appropriate combinations of non-zero values of the parameters. The next step is to calculate interference-free derivatives for the tapered wing by correcting derivatives measured in the tunnel with ventilations sealed. Equations (5) with appropriate values of the equivalent upwash parameters

† Some difficulty was encountered in the calculation of the steady streamline curvature parameter $\delta_1$ because the equations were ill-conditioned. Values were therefore interpolated using the relation

$$(\delta_1)_p = (\delta_1)_s - \frac{[(\delta_0)_s - (\delta_0)_p][(\delta_1)_s - (\delta_1)_{os}]}{(\delta_0)_s - (\delta_0)_{os}}$$

where suffix $p$ denotes perforated slots, $s$ denotes sealed slots and $os$ denotes open slots.

| | 0·16 cm (0·06 in) Perforations | 0·79 cm (0·31 in) Perforations |
|---|---|---|
| $\delta_0$ | 0·071 | −0·020 |
| $\delta_1$ | 0·330 | 0·014 |
| $\delta'_0$ | 0·011 | 0·082 |

tabulated above are then used to correct derivatives in the tunnel with 0·16 cm (0·06 in) and 0·79 cm (0·31 in) perforations behind the slots. Derivatives corrected in this way are seen to compare closely with the calculated interference-free curves in Figs. 11 to 14. In particular, with the perforations chosen to give small interference on stiffness for the half-delta wing (0·79 cm holes) Figs. 11 and 12 show that the significant residual interference on damping for the tapered half-wing can be corrected; similarly, with perforations chosen to give small interference on damping for the half-delta wing, Figs. 13 and 14 show that the residual interference on stiffness for the tapered half-delta wing can be corrected.

The half-delta wing and the unswept tapered wing both had a span equal to approximately 40 per cent of the tunnel width. Equations (5) were formulated for a small wing and calculations have shown that allowance for the finite span of the models reduces the interference parameters in a slotted tunnel by about 20 per cent. It follows that if a model with substantially different span from the half-delta wing is tested in the modified tunnel, the calculated corrections may be slightly in error.

## 7. Conclusions

1. Tests were made at reduced frequencies $\bar{\nu} < 0{\cdot}15$ on a half-wing of cropped-delta planform in a transonic tunnel which had ventilated walls consisting of perforated screens fitted behind longitudinal slots. It is found that values of pitching moment and lift derivatives vary systematically as the porosity of the screens is changed, giving sets of nearly parallel curves against Mach number from values with slots sealed to values with 'ideal' (open) slots.

2. A suitable choice of porosity of the walls by the method suggested in the text, offers a practical means of reducing the large ventilated wall effects on dynamic measurements. The method requires the use of the linearized theory of Ref. 1 to correct derivatives measured at subsonic speeds in the tunnel with ventilations sealed, and approximations in this theory appear to be the main limitation on the accuracy to which interference-free derivatives can be obtained.

3. Different ventilated wall conditions are required for interference-free damping and interference-free stiffness derivatives. Since the effects on the latter are usually small compared with the interference on damping, it is suggested that the ventilated walls are designed for interference-free damping and small corrections should then be applied to measured stiffness derivatives.

4. It has been shown in Ref. 2 that, when large interference effects are present at subsonic speeds, they persist throughout the transonic speed range although the mechanism producing supersonic interference is fundamentally different from that at subsonic speeds. The chosen interference-free ventilated walls for the present measurements, successfully reduce the large interference on damping at all speeds achieved in the tests, $0{\cdot}4 \leqslant M \leqslant 1{\cdot}05$.

5. Some tests have been done with a second half-wing with an unswept tapered planform. It is found that when the ventilated walls are adjusted to give interference-free derivatives for the model with cropped-delta planform, then only small interference effects are measured on the tapered wing which was subject to large wall interference when tested in a conventional slotted tunnel.

6. The porosity of the slotted-perforated walls is described by a parameter $P_E$ which relates the mass flow through the wall to the pressure drop across it. Values of $P_E$ measured for various wall conditions between the two extremes of sealed walls and open slots showed that for $M > 0{\cdot}6$, $P_E$ was nearly inde-

pendent of Mach number. It is suggested that with solely perforated walls, this Mach number independence may only be achieved if some perforations are sealed in longitudinal slots.

7. The slot parameter for the ventilated walls had the value 0·233. It is shown that small interference should be achieved respectively on damping derivatives and on stiffness derivatives when the porosity parameter $P_E$ for the slotted-perforated walls has the values 0·5 and 2·7 for the effective ratio 2·6 of tunnel breadth to height.

**Acknowledgement**

The authors wish to acknowledge the assistance of Mrs. J. A. Moreton of Aerodynamics Division NPL, who processed the measurements and also wrote the ALGOL programme used to determine corrections for wall interference.

## LIST OF SYMBOLS

| | |
|---|---|
| $A$ | aspect ratio |
| $b$ | effective breadth of tunnel working section |
| $\bar{c}$ | geometric mean chord of model half-wing |
| $C$ | cross-sectional area of tunnel working section $= \frac{1}{2}bh$ |
| $\bar{C}_L$ | (complex lift)/$q_\infty S$ |
| $\bar{C}_m$ | (complex pitching moment)/$q_\infty S\bar{c}$ |
| $F$ | slot parameter defined in equation (A2) |
| $h$ | height of tunnel working section |
| M | Mach number |
| $p$ | local static pressure |
| $P_\infty$ | static pressure of undisturbed stream |
| $P_E$ | porosity parameter for slotted-perforated walls used in the analysis of the experimental results (equation (1)) |
| $P$ | porosity parameter for viscous slot flow (equation (A8)) |
| $P_I$ | porosity parameter for a perforated wall (equation (A11)) |
| $\Delta p$ | pressure drop across the ventilated wall |
| $q_\infty$ | dynamic pressure of undisturbed stream |
| $S$ | area of model half-wing |
| $u$ | perturbation velocity in the direction of the undisturbed stream |
| $U_\infty$ | velocity of the undisturbed stream |
| $v_n$ | velocity normal to the ventilated wall |
| $x_0$ | streamwise distance of the pitching axis from the root leading edge |
| $z_0$ | amplitude of heaving oscillation |
| $\beta$ | $(1 - \mathrm{M}^2)^{\frac{1}{2}}$ |
| $\delta_0$ | steady upwash interference parameter } defined in Ref. 1 |
| $\delta_1$ | steady streamline curvature parameter } defined in Ref. 1 |
| $\delta_0'$ | unsteady upwash interference parameter } defined in Ref. 1 |
| $\theta_0$ | amplitude of pitching oscillation |
| $\Psi$ | $(1 + 1/P_E)^{-1}$ |
| $\bar{\nu}$ | reduced frequency parameter $= \omega\bar{c}/U_\infty$ |
| $\rho$ | local density of stream |
| $\rho_\infty$ | density of undisturbed stream |
| $\phi$ | perturbation velocity potential |

$\omega$ angular frequency of oscillation

*Derivatives*

The non-dimensional derivatives of lift $l_\theta$, $l_{\dot\theta}$, $l_z$, $l_{\dot z}$ are defined by

$$\bar{C}_L = 2\theta_0(l_\theta + i\bar{v}l_{\dot\theta}) + 2\frac{z_0}{\bar{c}}(l_z + i\bar{v}l_{\dot z})$$

The non-dimensional derivatives of pitching moment $m_\theta$,$m_{\dot\theta}$, $m_z$, $m_{\dot z}$ are defined by

$$\bar{C}_m = 2\theta_0(m_\theta + i\bar{v}m_{\dot\theta}) + 2\frac{z_0}{\bar{c}}(m_z + ivm_{\dot z}).$$

## REFERENCES


| *No* | *Author(s)* | *Title, etc.* |
|---|---|---|
| 1 | H. C. Garner, A. W. Moore and K. C. Wight .. .. | The theory of interference effects on dynamic measurements in slotted-wall tunnels at subsonic speeds and comparisons with experiment. A.R.C. R. & M. 3500. September, 1966. |
| 2 | A. W. Moore and K. C. Wight | An experimental investigation of wall interference effects on dynamic measurements on half-models in ventilated tunnels through the transonic speed range. A.R.C. R. & M. 3570. August, 1967. |
| 3 | B. H. Goethert .. .. | Transonic Wind Tunnel Testing. AGARDograph 49. Pergamon Press. 1961. |
| 4 | A. W. Moore and K. C. Wight | On achieving interference-free results from dynamic tests on half models in transonic wind tunnels. A.R.C. R. & M. 3636. March, 1969. |
| 5 | G. Q. Hall and J. S. Claridge | Measurements of flow distriburbances caused by an oscillating wing in a slotted wall tunnel. H.S.D./Cov. A.R.L. Report No. 66/4. October, 1966. |
| 6 | B. S. Baldwin, J. B. Turner and E. D. Knetchtel .. .. | Wall interference in wind tunnels with slotted and porous boundaries at subsonic speeds. N.A.C.A. T.N. 3176. May, 1954. |
| 7 | T. R. Goodman .. .. | The porous wall wind tunnel. Part II. Interference effect on a cylindrical body in a two-dimensional tunnel at subsonic speed. Cornell Aeronautical Lab. Report No. A.D-594-A-3. November, 1950. |
| 8 | P. F. Maeder .. .. .. | Investigation of the boundary condition at a perforated wall. Brown University Divn. of Engineering. Tech. Report WT-9. May, 1953. |

## Appendix

### Boundary Condition for a Slotted-Perforated Wall

As noted in Section 4 of the paper it is desirable to formulate a boundary condition for the slotted-perforated wall in order to generalize the approach adopted in the experiments. It is also desirable to find a basis for comparison between interference due to an 'ideal' slotted-perforated wall (i.e., with inviscid flow) and interference when viscous slot flow is important. In both cases the porosity of the boundary influences the interference upwash in the tunnel, but the porosity of an ideal perforated wall relates the mass flow through the wall to the pressure drop across it in inviscid flow, whilst the effective porosity of a slotted wall is significant only when viscous flow at the boundary is predominant, e.g., when slot width is less than the boundary-layer displacement thickness. The porosity due to viscous slot flow can be associated with that of a truly porous wall, and one might expect a similar porosity effect for a perforated wall if the perforation size is less than the boundary-layer displacement thickness.

When the ventilations consist only of longitudinal slots it is well known that, provided viscous effects in the slots are negligible, the slotted wall in steady flow may be treated by a homogeneous condition

$$\phi + K\frac{\partial \phi}{\partial n} = 0, \tag{A1}$$

where $\phi$ is the perturbation velocity potential, $n$ denotes the outward normal distance from the boundary, and for slots of width $a$ and periodic spacing $d$ in the tunnel of height $h$ the constant $K$ is given by the non-dimensional slot parameter

$$F = \frac{2K}{h} = \frac{2d}{\pi h}\log_e \operatorname{cosec}\frac{\pi a}{2d}. \tag{A2}$$

Equation (A2) also holds for oscillatory flow, but it has been found[1] that slotted-wall interference is significantly changed when there are appreciable viscous effects in the slots. A boundary condition for steady flow has been proposed by Baldwin, Turner and Knechtel[6], and we write this as

$$\frac{\partial \phi}{\partial x} + K\frac{\partial^2 \phi}{\partial x\,\partial n} + G\frac{\partial \phi}{\partial n} = 0, \tag{A3}$$

where $G$ is a general parameter which describes the porosity of the ventilated wall. Assuming that viscous slot flow is similar to the flow at a truly porous wall, parameter $G$ may be written

$$G = \frac{1}{P} \tag{A4}$$

where $P$ is a porosity parameter which, following Goodman[7], relates the pressure drop across the wall to the outflow. The pressure drop across a porous wall is given by Darcy's law

$$\Delta p \propto v_n. \tag{A5}$$

When Bernoulli's equation in compressible flow is linearized, the same relation is obtained as for incompressible flow, namely

$$\Delta p = \rho_\infty U_\infty u \tag{A6}$$

where $\rho_\infty$, $U_\infty$ are the density and velocity of the undisturbed flow, and $u$ is the perturbation velocity in the stream direction. Goodman obtains the boundary condition at the porous wall from equations (A5) and (A6) as

$$\frac{u}{U_\infty} = \frac{1}{P}\frac{v_n}{U_\infty} \tag{A7}$$

where parameter $P$ is given by

$$\frac{\Delta p}{q_\infty} = \frac{2}{P}\frac{v_n}{U_\infty}, \tag{A8}$$

$q_\infty$ being the dynamic pressure $\frac{1}{2}\rho_\infty U_\infty^2$. Baldwin, Turner and Knechtel calculate the interference in a tunnel with walls represented by boundary condition (A3) with $G = 1/P$; after application of the Prandtl–Glauert transformation, they find that the relevant parameter describing interference effects due to the finite porosity of the slots is $\beta/P$, where $P$ is defined is equation (A8). This implies that, with finite non-zero values of $P$, viscous flow effects tend to zero as sonic speed is approached and interference appropriate to ideal slotted boundaries is obtained. Some experimental evidence reported in Ref. 1 supports this conjecture. Dynamic tests were done in a transonic tunnel with roof and floor containing slots which were narrower than the boundary-layer displacement thickness. At low subsonic speeds, values of pitching damping with slots open were close to the values measured with slots sealed although a substantial difference was predicted on the assumption of ideal slot flow. This behaviour was probably due to the significant viscous effects at the slotted wall which could give a large value of parameter $\beta/P$. However, Figs. 20 and 21 of Ref. 1 suggest that, as the speed was increased beyond M = 0·8 so that $\beta/P$ was decreasing, the measured pitching damping tended to move towards the values predicted for ideal slotted walls.

Physically, the effect of viscosity might be regarded as a resistance to outflow at the slotted wall. It has been suggested[3] that perforated screens fitted over the slots in inviscid flow would produce a similar resistance to outflow—the ventilated walls used in the present tests are basically of this form. To determine a porosity parameter for the slotted-perforated walls in inviscid flow, consider first the boundary condition for a perforated wall. Assuming that an idealized perforated wall consists of an infinite number of traverse slots, Maeder[8] shows that in incompressible flow the relation between the perturbation velocity in the stream direction and the velocity normal to the wall is

$$\frac{v_n}{U_\infty} = P_I \frac{u}{U_\infty} \tag{A9}$$

where $P_I$ is a constant for a given wall configuration. In (A9), $v_n/U_\infty$ represents slat incidence, and $u/U_\infty$ represents normal force coefficient or pressure. Compressibility increases the ratio force coefficient/incidence and hence $u/v_n$ by the factor $\beta^{-1}$. The boundary condition for compressible flow past the idealized perforated wall is therefore

$$\frac{v_n}{U_\infty} = \beta P_I \frac{u}{U_\infty}. \tag{A10}$$

Equation (A6) may again be applied so that $P_I$ can be defined by the expression

$$\frac{\Delta p}{q_\infty} = \frac{2}{\beta P_I} \frac{v_n}{U_\infty}. \tag{A11}$$

Hence, it is reasonable to assume that the boundary condition for inviscid flow at a slotted wall with perforations over the slots has the form given by equation (A3) with

$$G = 1/\beta P_I. \tag{A12}$$

It follows from equations (A4) and (A12) that the boundary condition for inviscid flow at an idealized slotted-perforated wall and the boundary condition for viscous flow through a slotted wall are identical with incompressible flow ($\beta = 1$), but with compressible flow the equations only have the same form if

$$\beta P_I = P. \tag{A13}$$

Since Baldwin et al find that interference effects are proportional to $\beta/P$, one might expect that interference in a tunnel with perforations at the slots is proportional to $1/P_I$ and is therefore independent of Mach number.

In order to avoid the difficulty of dealing with equation (A11) when $\beta = 0$, a porosity parameter $P_E$ for the slotted-perforated walls used in the tests is defined using the relation

$$\frac{\Delta p}{q_\infty} = \frac{2}{P_E}\frac{v_n}{U_\infty}. \tag{A14}$$

The question arises with compressible flow as to how parameter $P_E$ relates to $P_I$ and hence, via equation (A13), to the parameter $P$ used in the theoretical treatment of viscous slot flow. At first sight, equations (A8) and (A14) seem to indicate directly that parameter $P_E$ is the same as parameter $P$, but this is not so. Parameter $P$ is defined specifically for viscous slot flow in equations (A7) and (A8), and interference effects are then proportional to $\beta/P$. As noted earlier in the Appendix, this implies that porosity effects become small as sonic speed is approached and curves plotted against Mach number for different wall porosities would collapse towards a single curve for an ideal slotted boundary. But the measured results with slotted-perforated walls discussed in Section 5 show no such trend; indeed the variation of the measured derivatives with parameter $P_E$ was found to be practically independent of Mach number at all speeds in the range $0{\cdot}6 \leqslant M \leqslant 1{\cdot}05$.

It is important to note that the present results show no effect of compressibility even with the 0·48 cm (0·19 in) and 0·79 cm (0·31 in) perforations which are considerably larger than the boundary-layer displacement thickness (approximately 0·28 cm (0·11 in) measured above a slat). Under these conditions there should be no appreciable viscous effects in the flow through the perforated wall, and the inviscid theoretical boundary condition should be applicable. Since there are no compressibility effects measured for tunnel main-stream speeds up to and including $M = 1{\cdot}05$, it appears that the flow within the slots at the perforated boundary of the present experiments remains incompressible. Therefore, setting $\beta = 1$ and comparing equation (A11) with equation (A14) we show that

$$P_E = P_I. \tag{A15}$$

It follows from equation (A13) that in comparisons of measured interference in the present tests and theoretical predictions for viscous slot flow, it is necessary to write

$$\beta P_E = P. \tag{A16}$$

Since the relevant parameter describing interference effects with viscous slot flow is $\beta/P$, wall constraint due to the slotted-perforated boundary should be related to $1/P_E$.

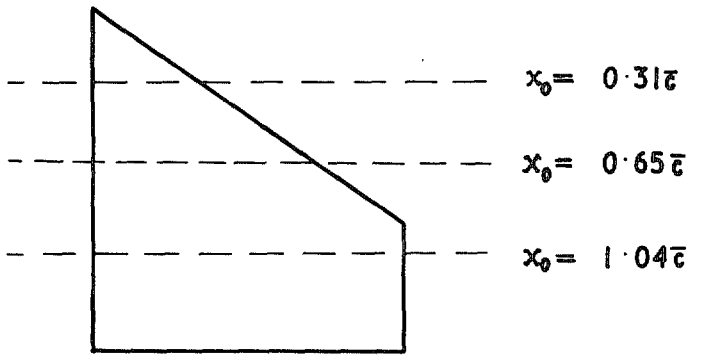


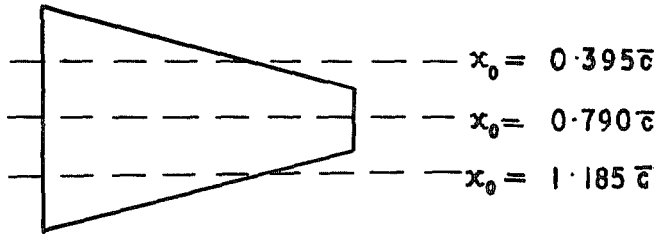


| | Delta wing | Tapered wing |
|---|---|---|
| Aspect ratio | 2·63 | 4·34 |
| Section | 6% RAE 102 | 5% Double wedge |
| Taper ratio | 0·389 | 0·267 |
| Span(½ model) | 3·61 in. (9·17 cm) | 3·60 in. (9·14 cm) |
| Root chord | 4·00 in.(10·16 cm) | 2·62 in. (6·65 cm) |
| Mean chord | 2·75 in.(6.99 cm) | 1·66 in. (4·22 cm) |
| L.E. sweepback | 33·7 deg. | 14·9 deg. |

FIG 1. Planforms and details of models

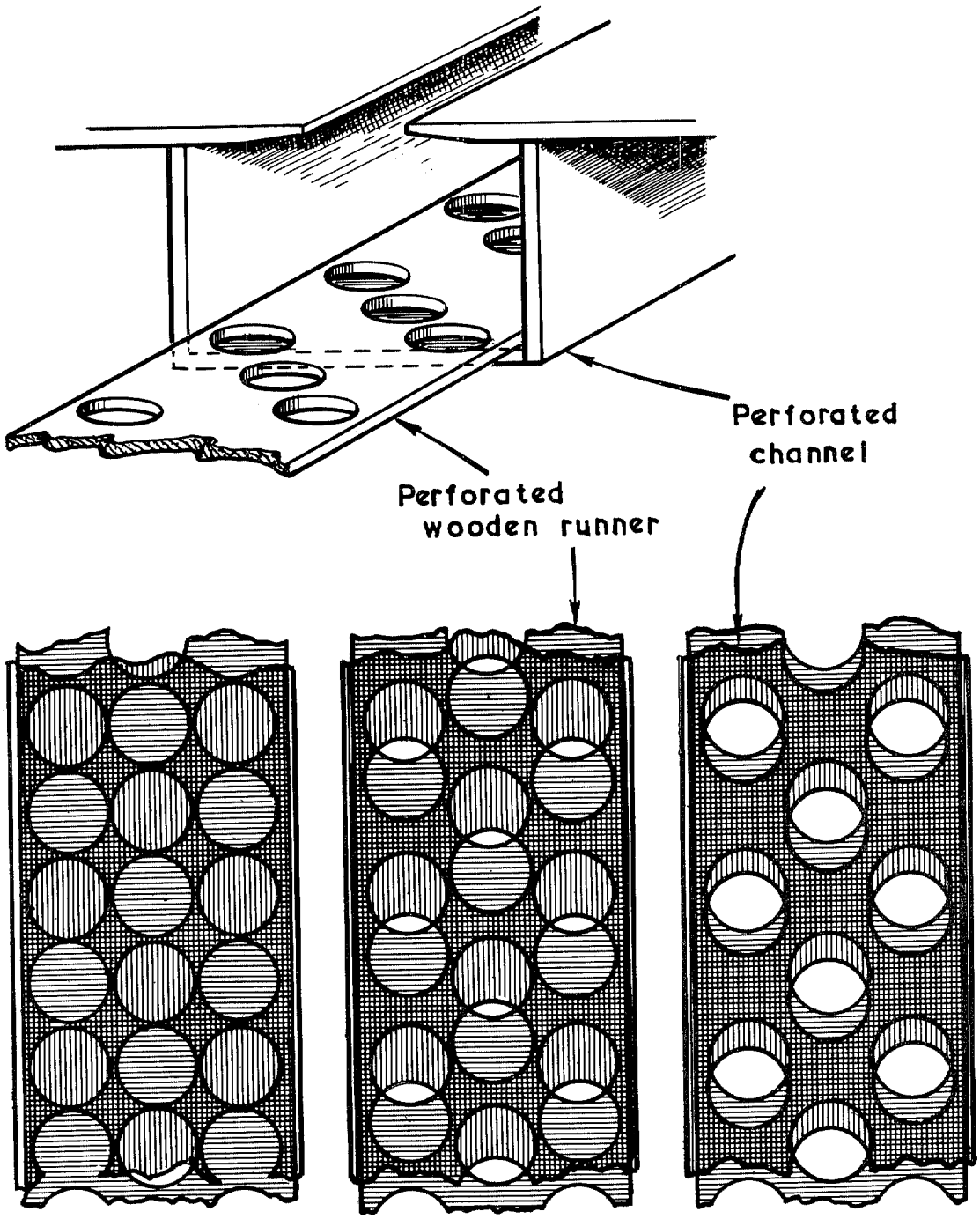


FIG. 2. Walls with variable porosity

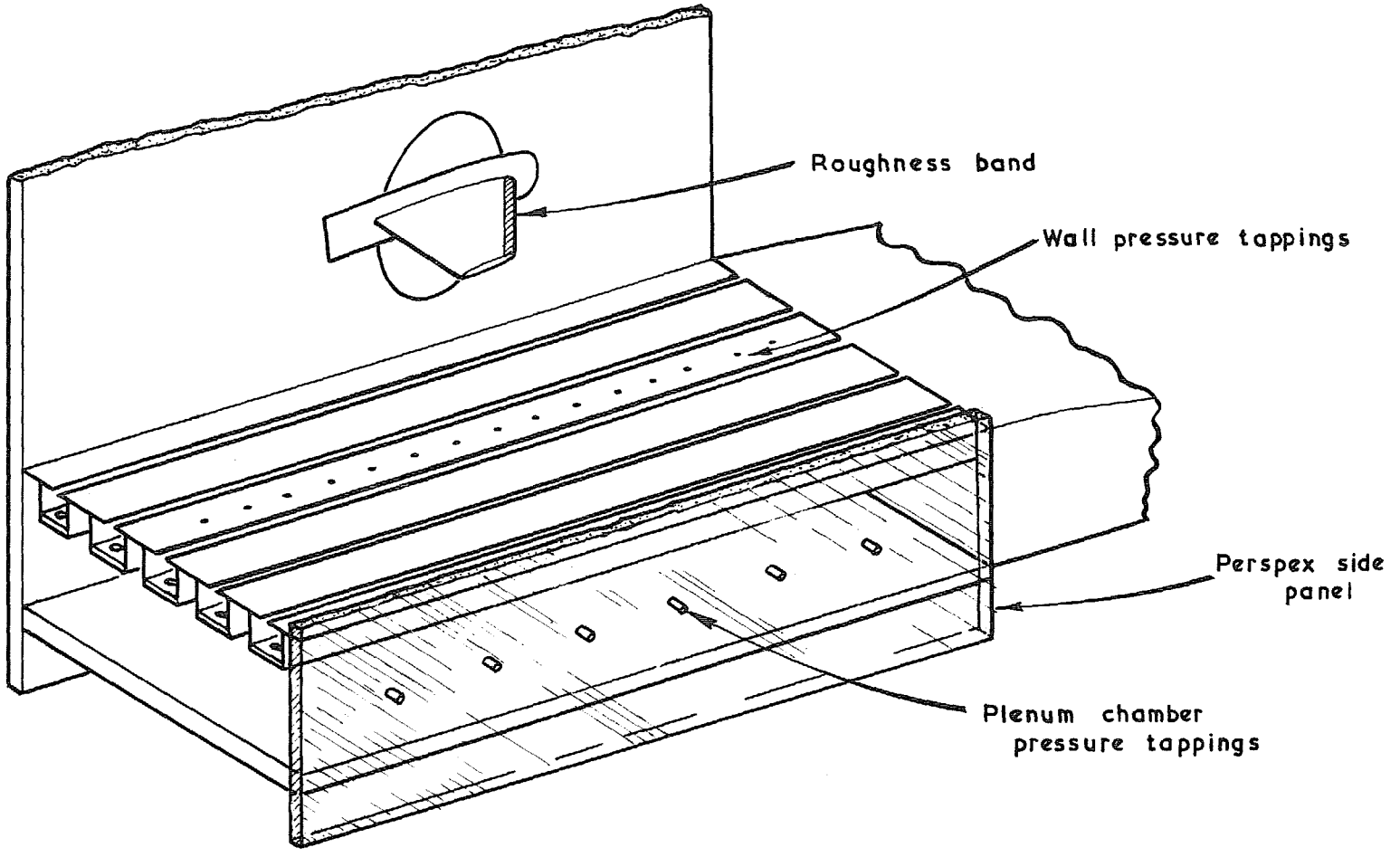


FIG. 3. Diagrammatic view of tunnel working section with modified walls

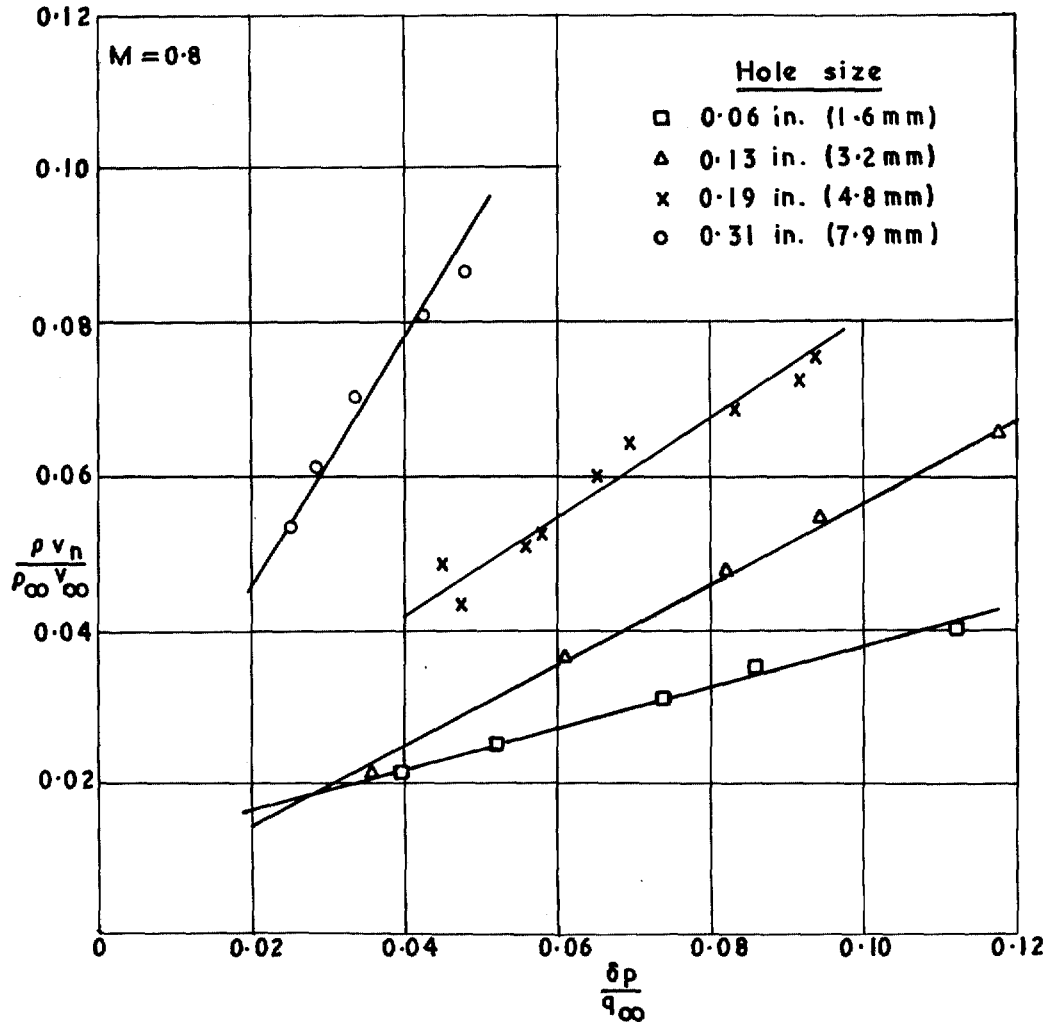


FIG. 4. Variation of mass flow through the slotted-perforated wall with pressure drop across it

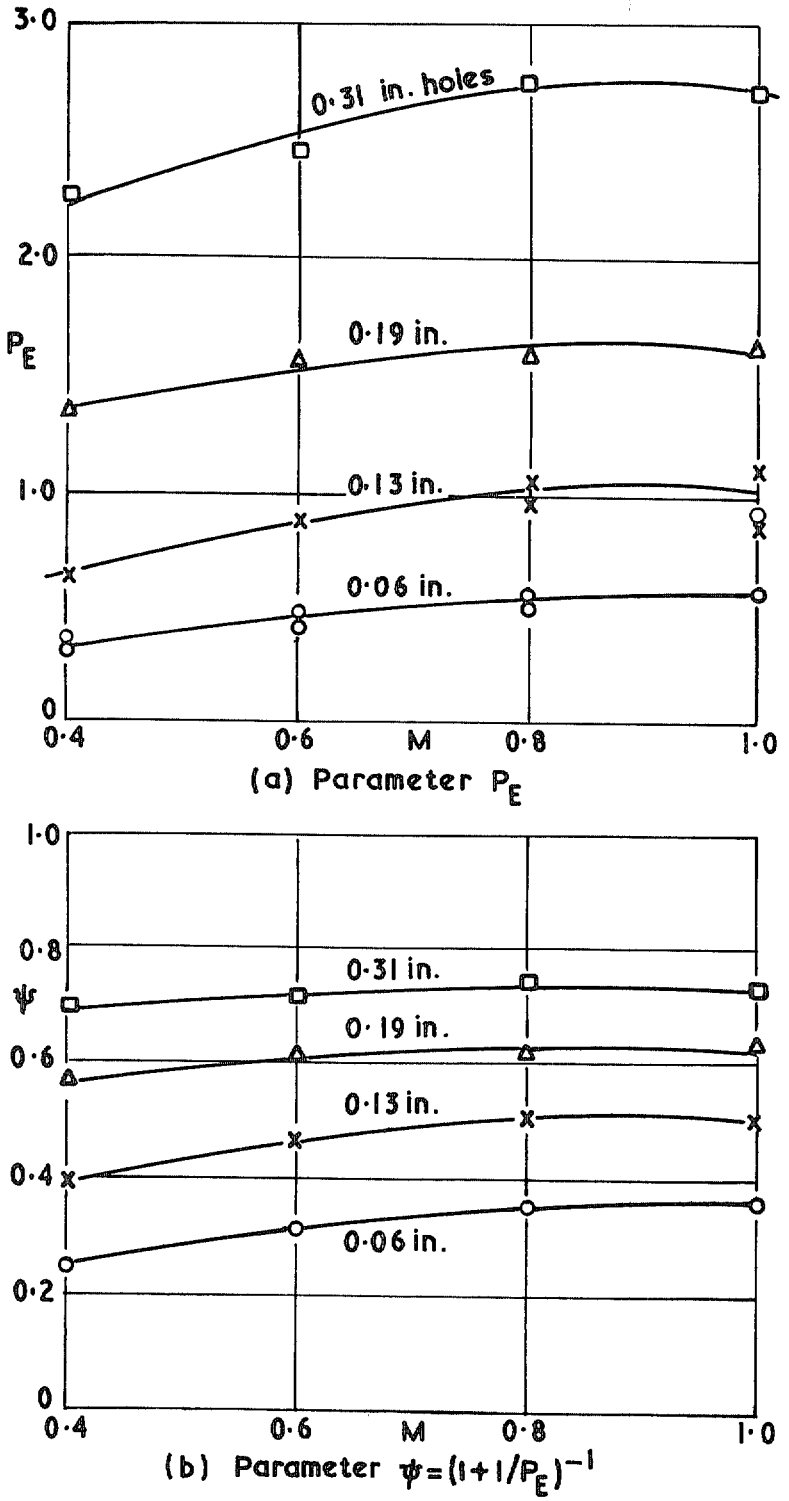


FIG. 5. Variation with Mach number of the porosity parameters for the slotted-perforated wall

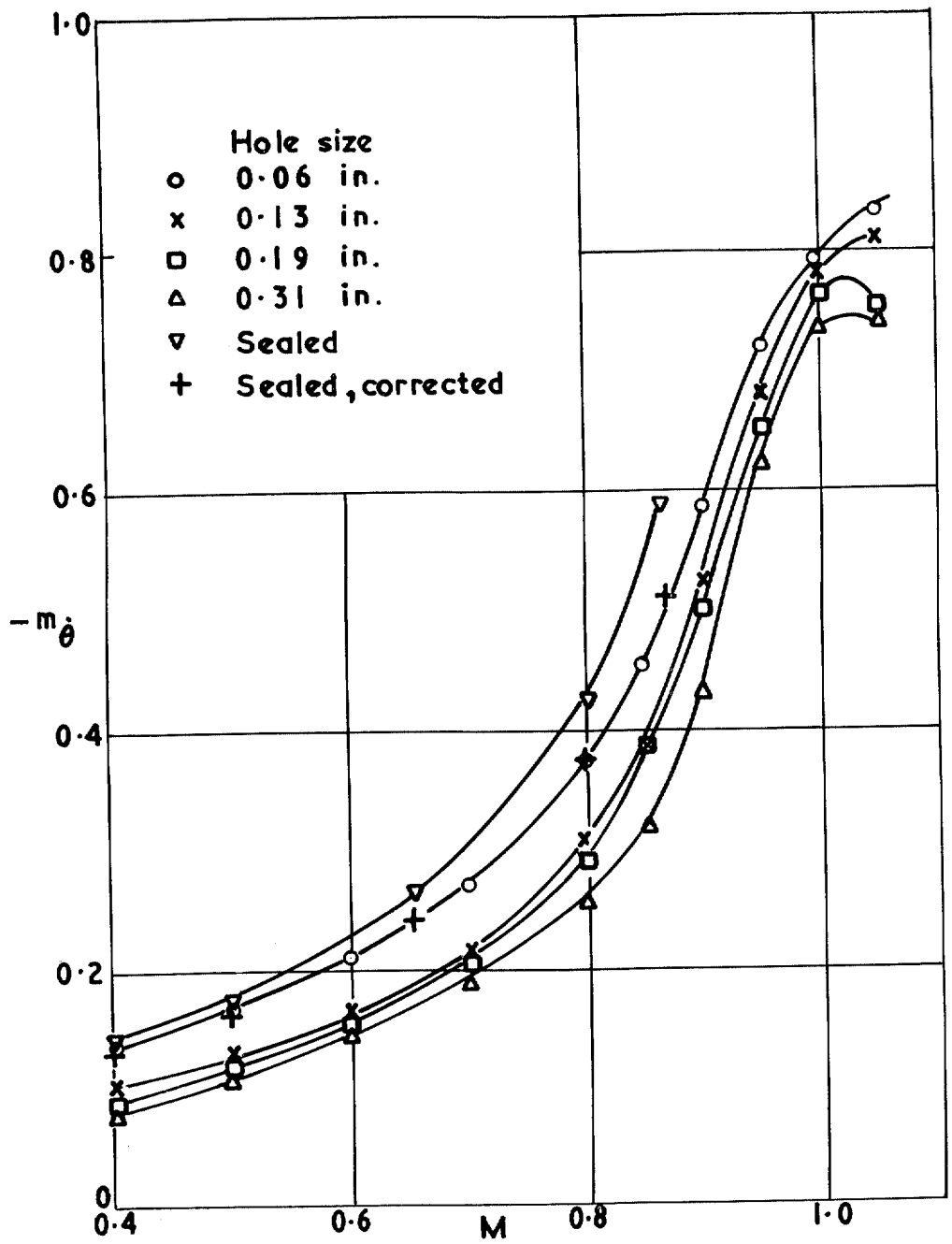


FIG. 6(a). Variation of derivative $m_{\dot{\theta}}$ with Mach number for the half-delta wing. $x_0 = 1{\cdot}04\,\bar{c}$

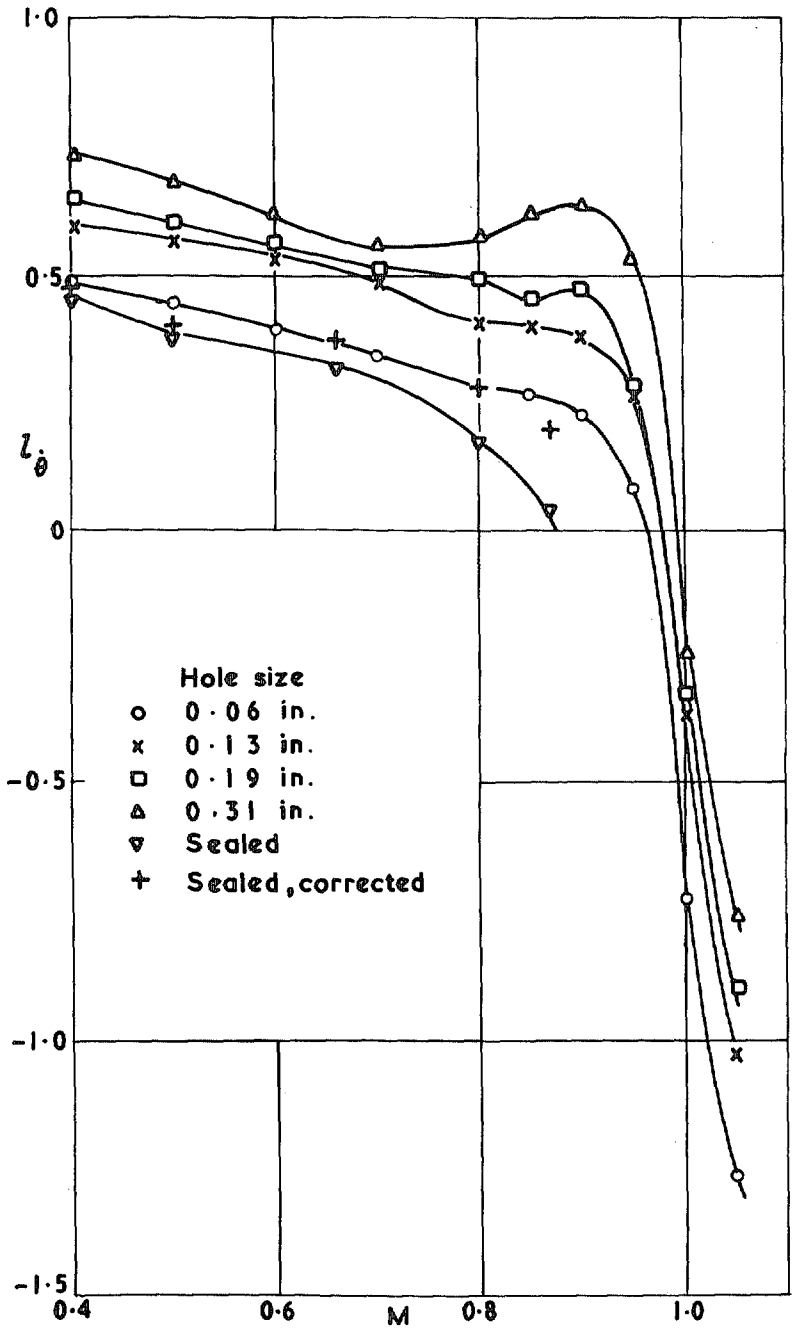


FIG. 6(b). Variation of derivative $l_{\dot{\theta}}$ with Mach number for the half-delta wing. $x_0 = 1{\cdot}04\,\bar{c}$

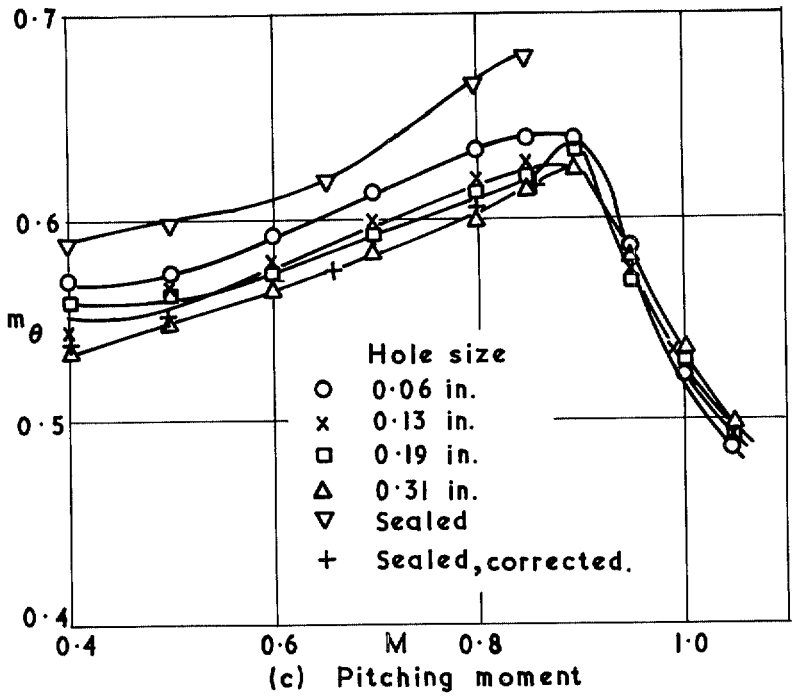


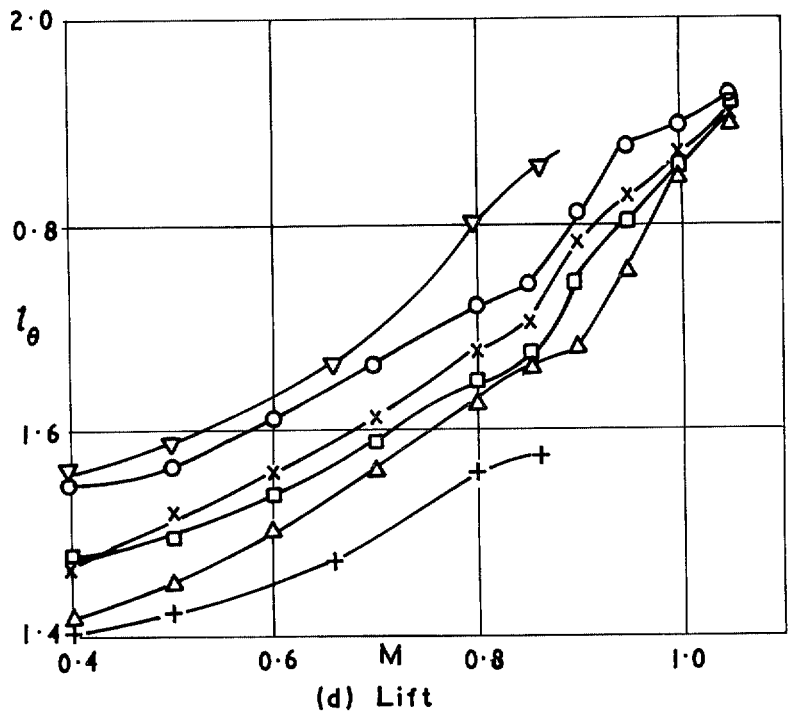


FIG. 6(c) and (d). Variation of stiffness derivatives with Mach number for the half-delta wing. $x_0 = 1{\cdot}04\ \bar{c}$

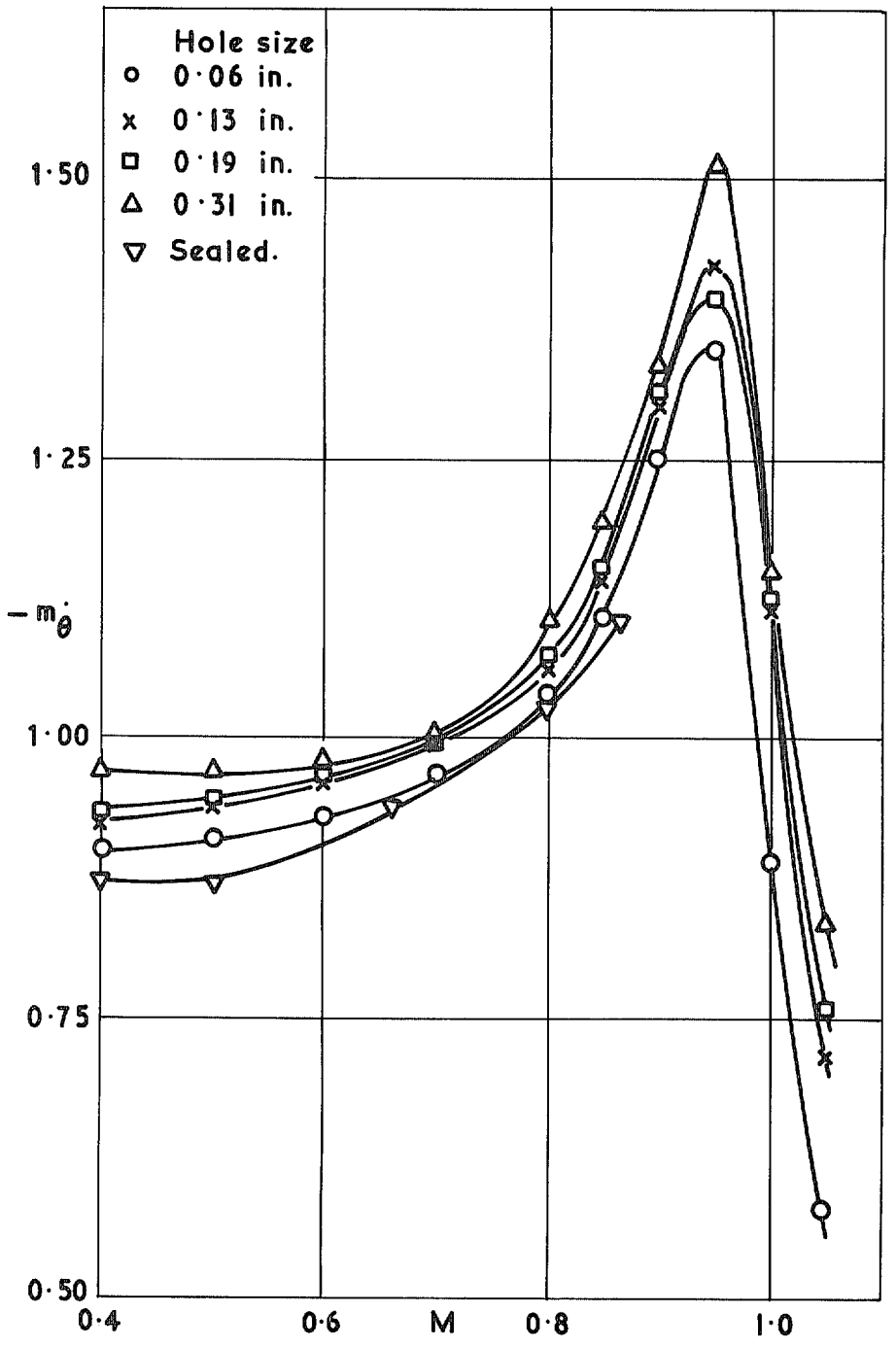


FIG. 7(a). Variation of derivative $m_{\dot{\theta}}$ with Mach number for the half-delta wing. $x_0 = 0{\cdot}31\,\bar{c}$

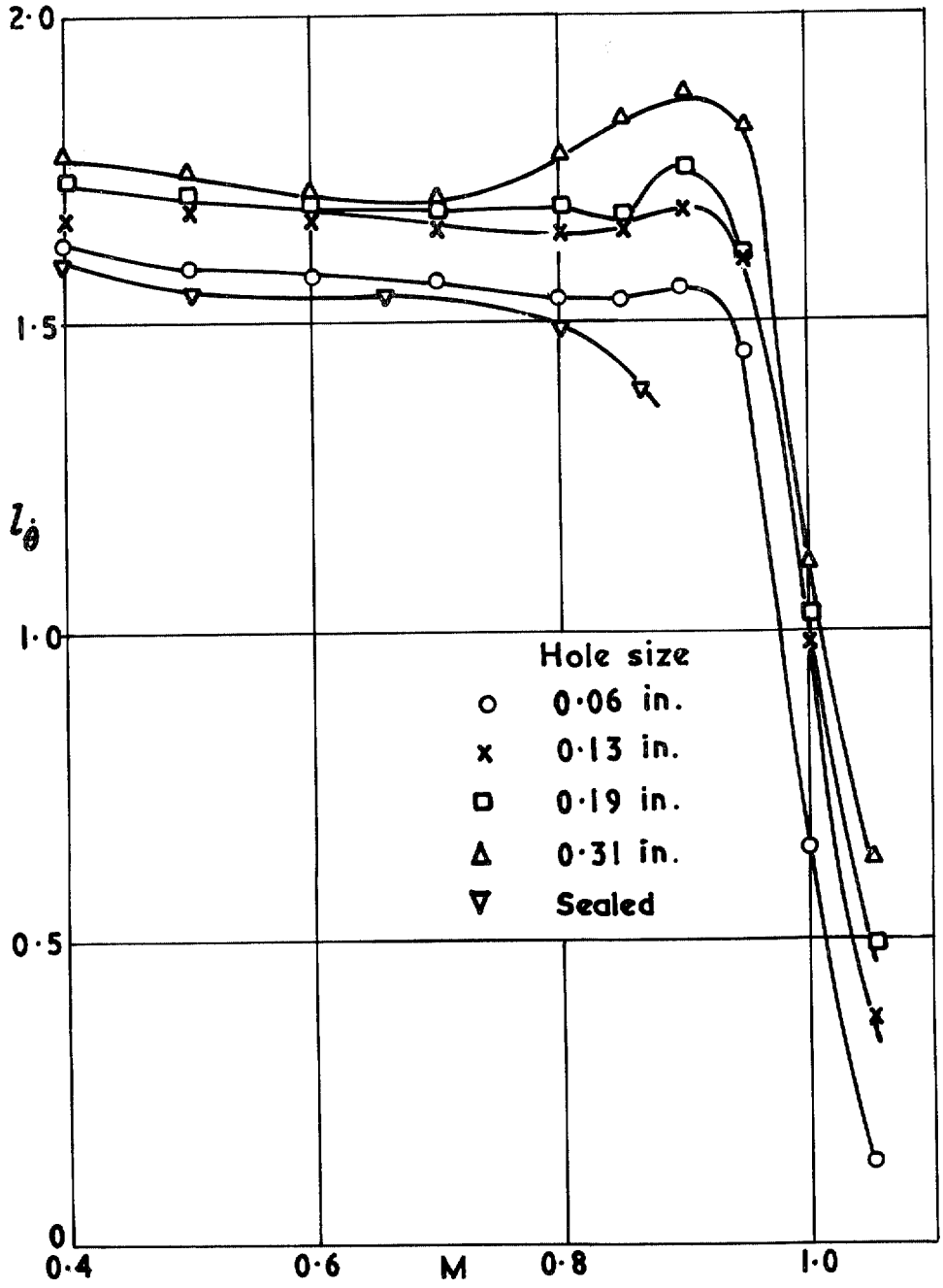


FIG. 7(b). Variation of derivative $l_{\dot{\theta}}$ with Mach number for the half-delta wing. $x_0 = 0{\cdot}31\,\bar{c}$

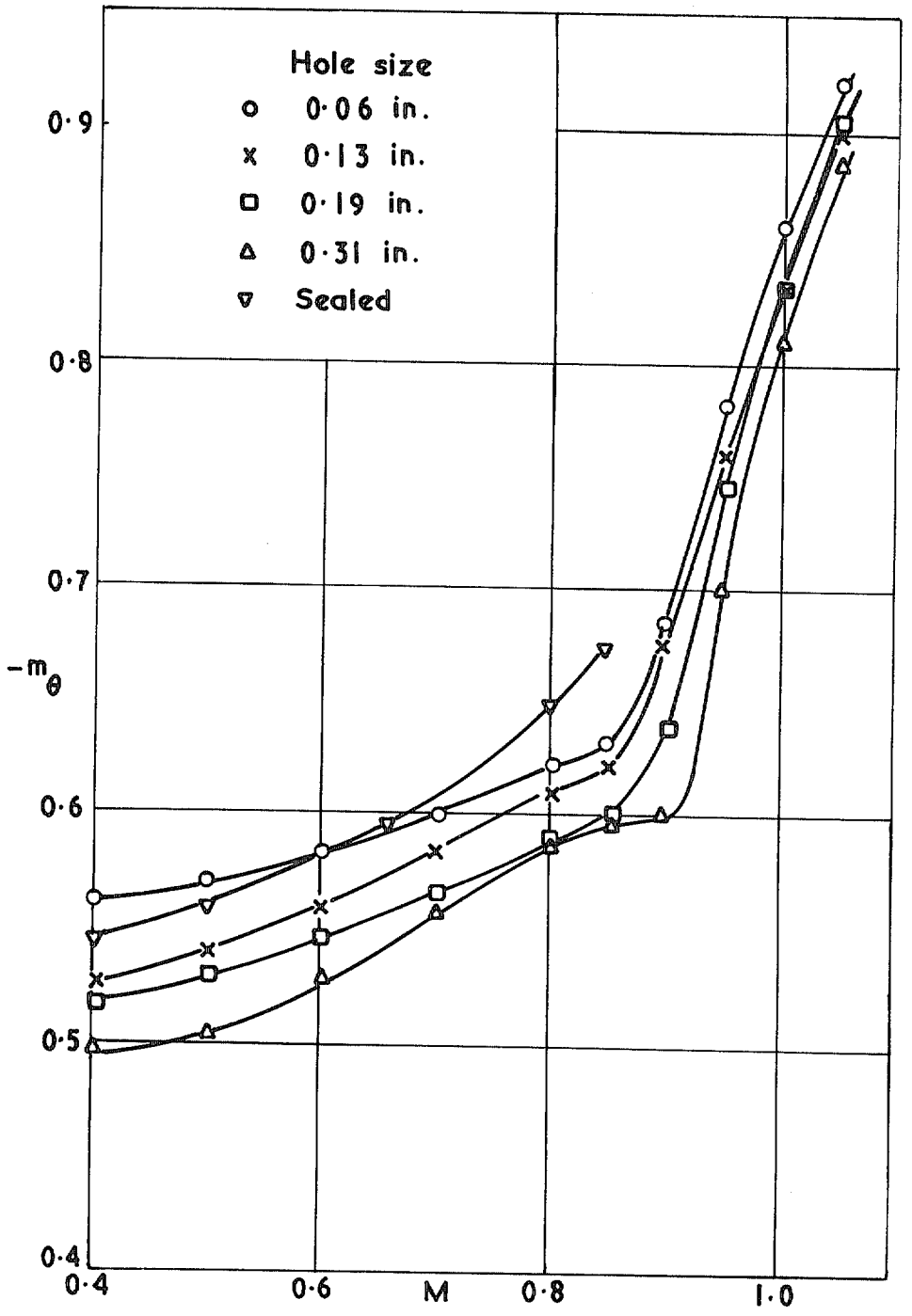


FIG. 7(c). Variation of derivative $m_\theta$ with Mach number for the half-delta wing. $x_0 = 0{\cdot}31\ \bar{c}$

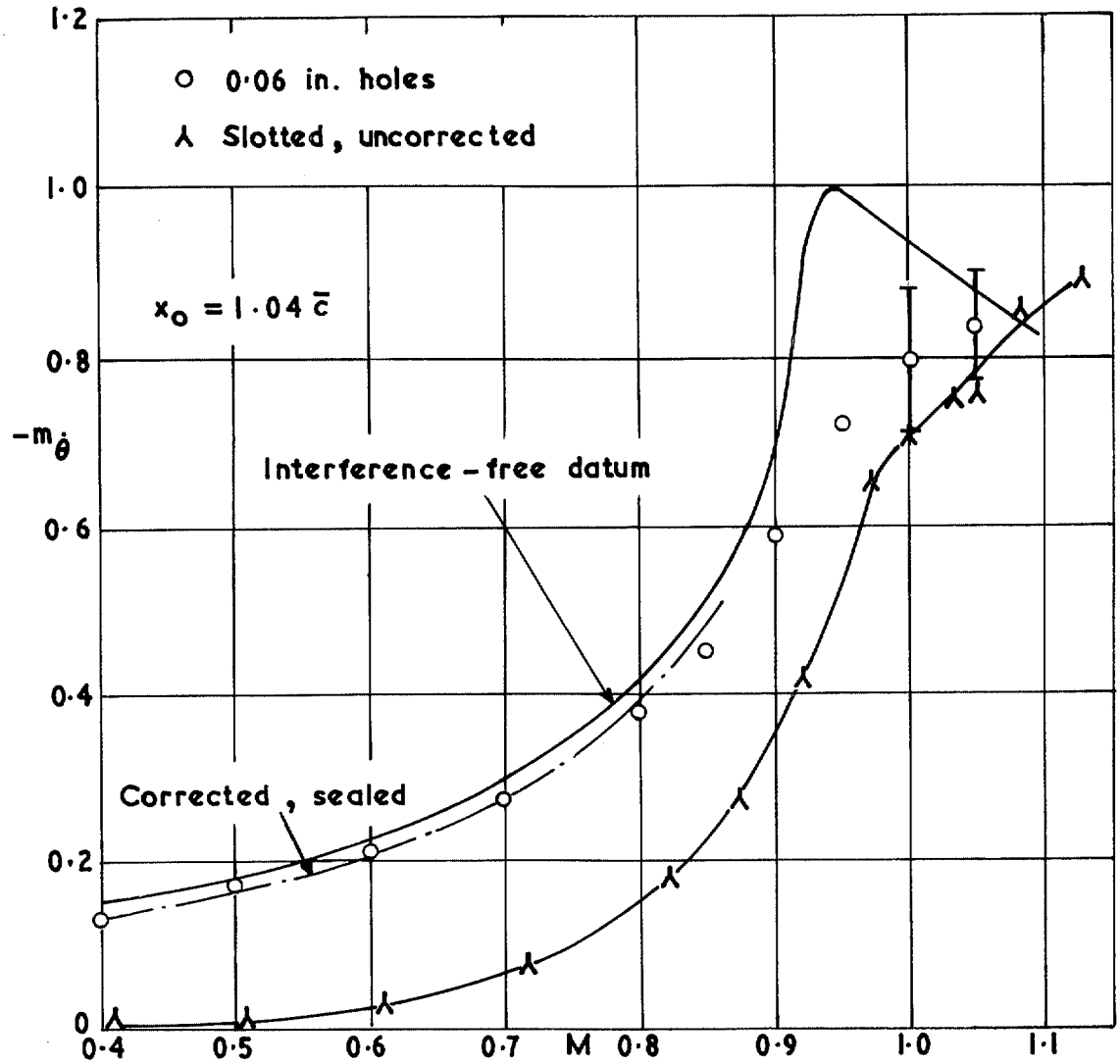


FIG. 8(a). Comparison of results from the $9\frac{1}{2}$ in × $9\frac{1}{2}$ in tunnel with interference-free values of pitching damping for the half-delta wing

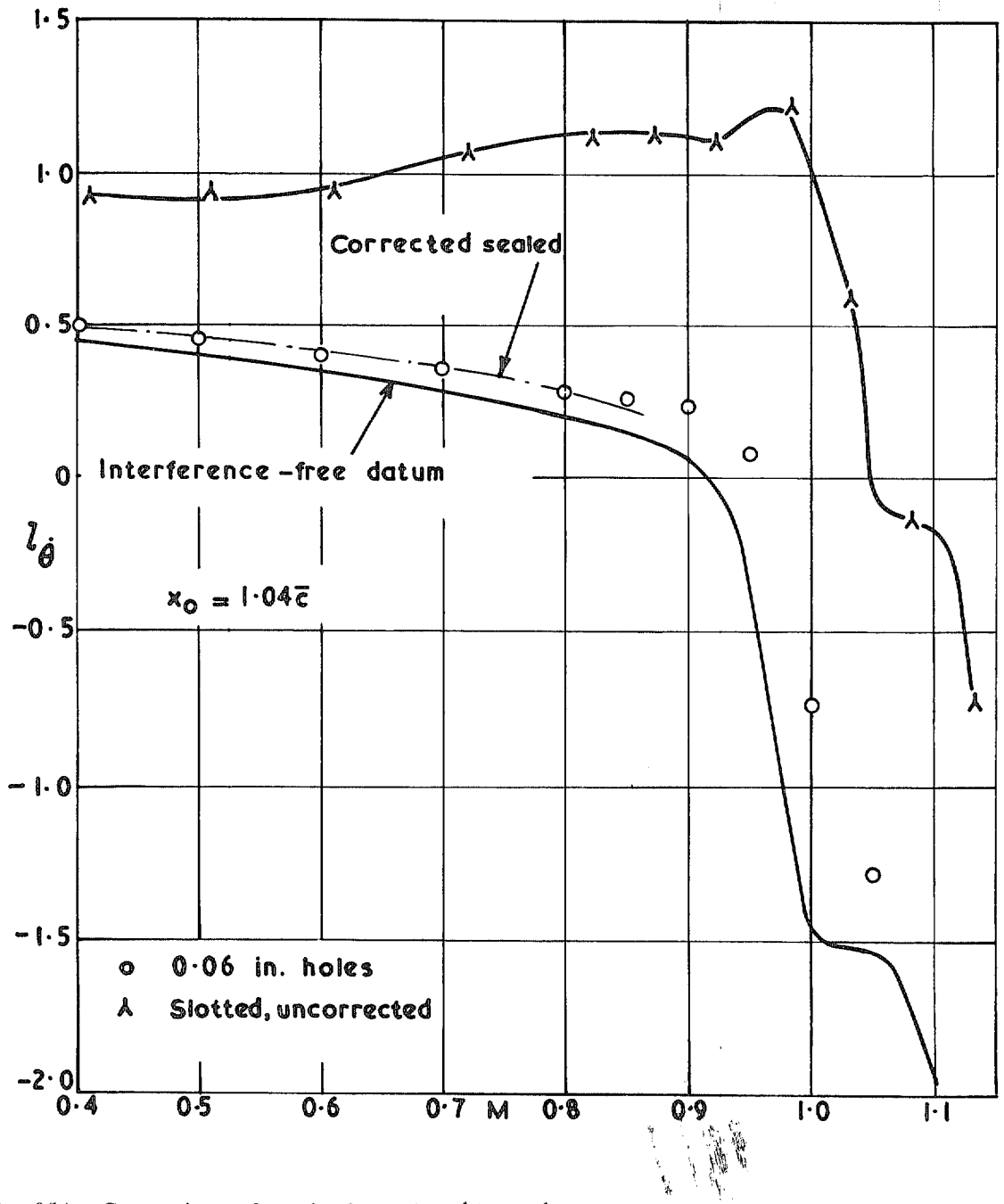


FIG. 8(b). Comparison of results from the $9\frac{1}{2}$ in × $9\frac{1}{2}$ in tunnel with interference-free values of lift derivative $l_{\dot{\theta}}$ for the half-delta wing

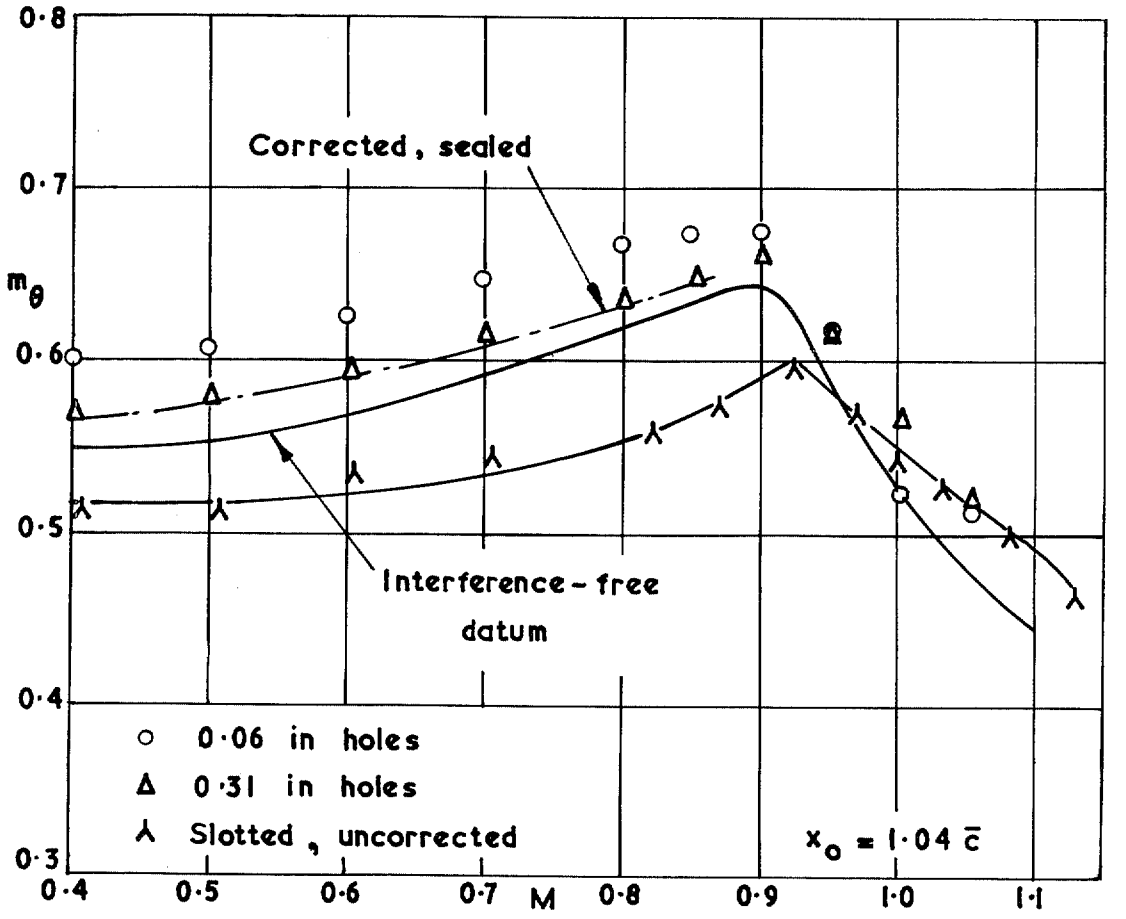


FIG. 8(c). Comparison of results from the $9\frac{1}{2}$ in × $9\frac{1}{2}$ in tunnel with interference-free values of pitching-stiffness for the half-delta wing

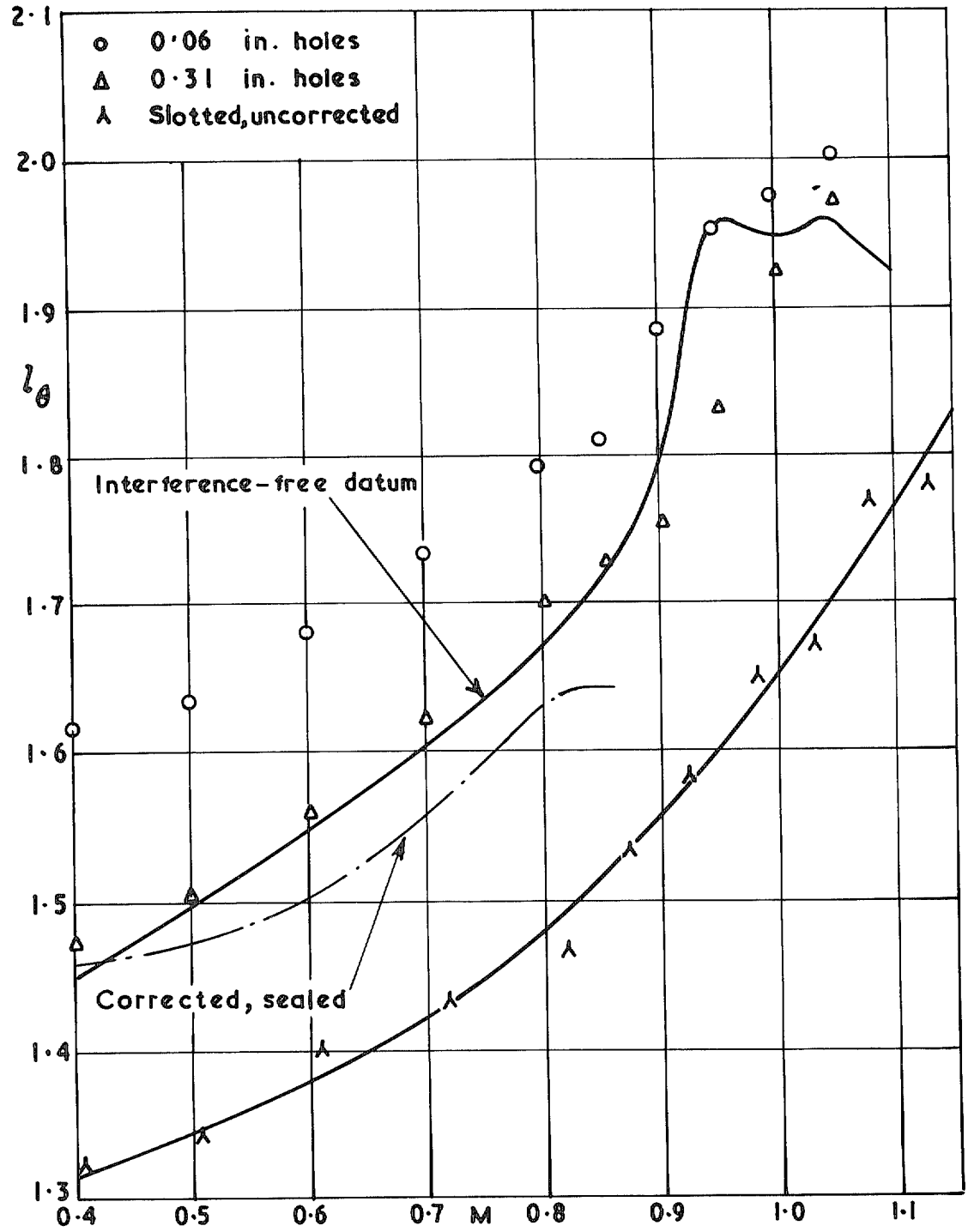


FIG. 8(d). Comparison of results from the $9\frac{1}{2}$ in × $9\frac{1}{2}$ in tunnel with interference-free values of lift derivative $l_\theta$ for the half-delta wing

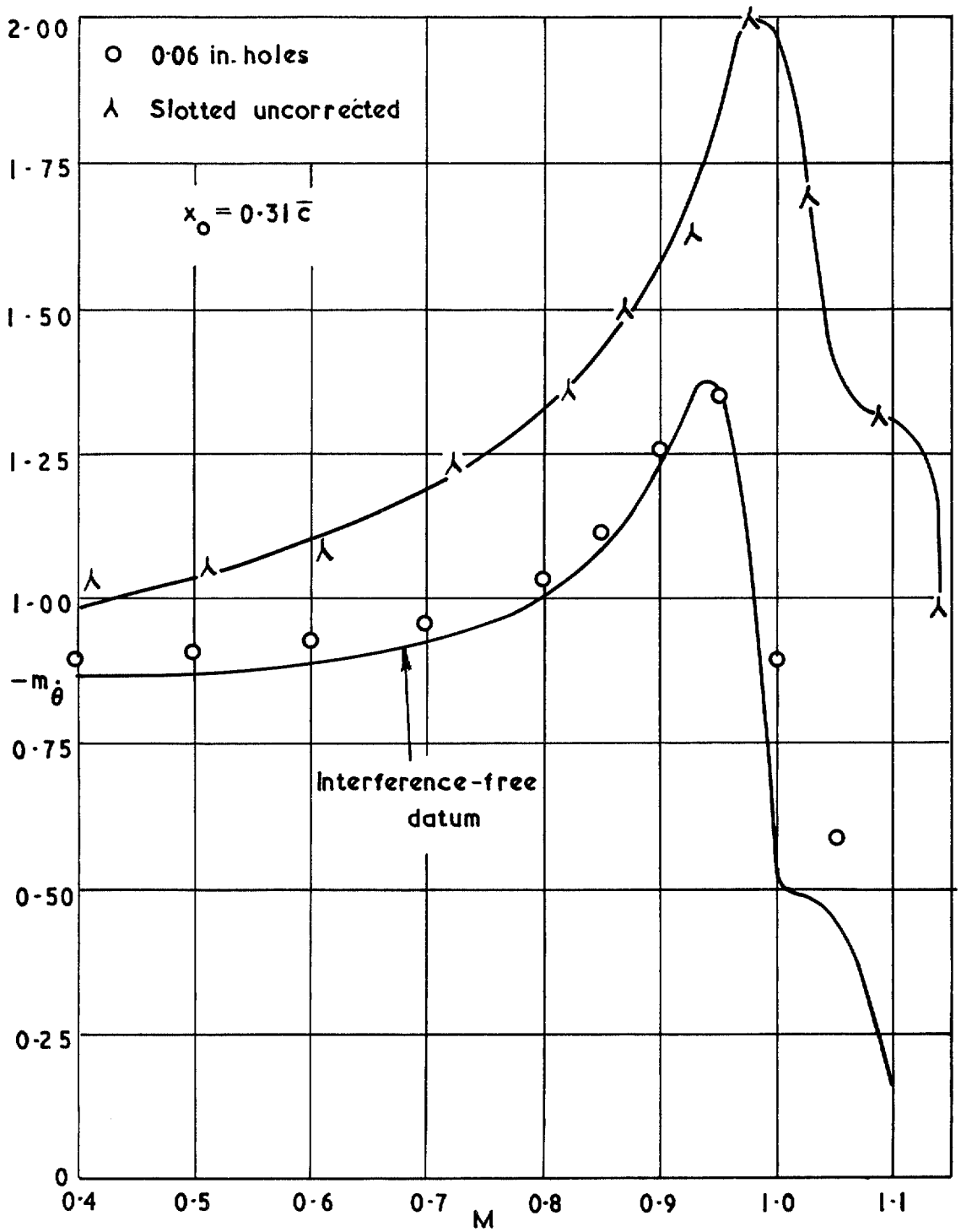


FIG 9(a). Comparison of results from the $9\frac{1}{2}$ in × $9\frac{1}{2}$ in tunnel with interference-free values of pitching damping for the half-delta wing

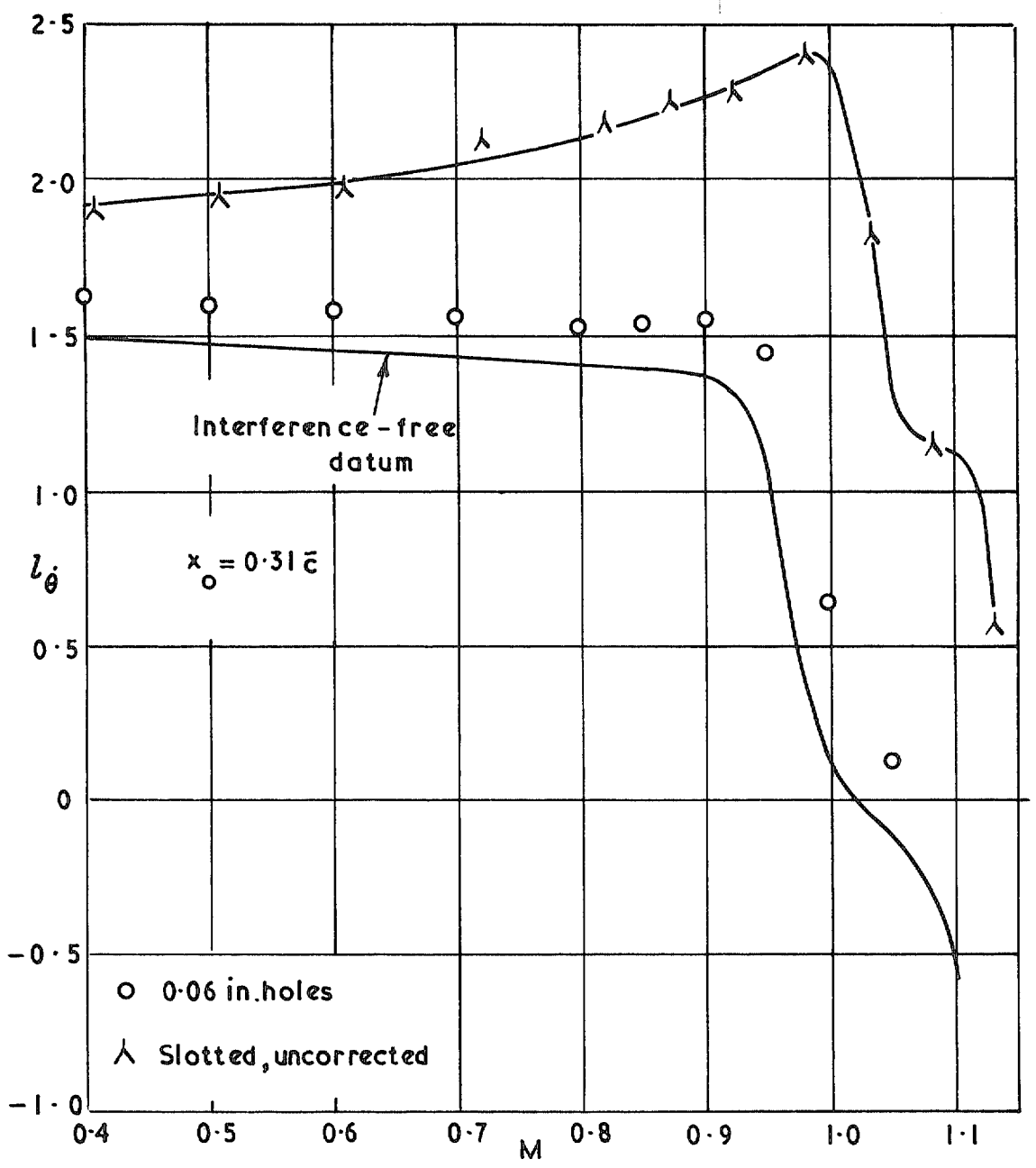


FIG. 9(b). Comparison of results from the $9\frac{1}{2}$ in × $9\frac{1}{2}$ in tunnel with interference-free values of lift derivative $l_{\dot{\theta}}$ for the half-delta wing

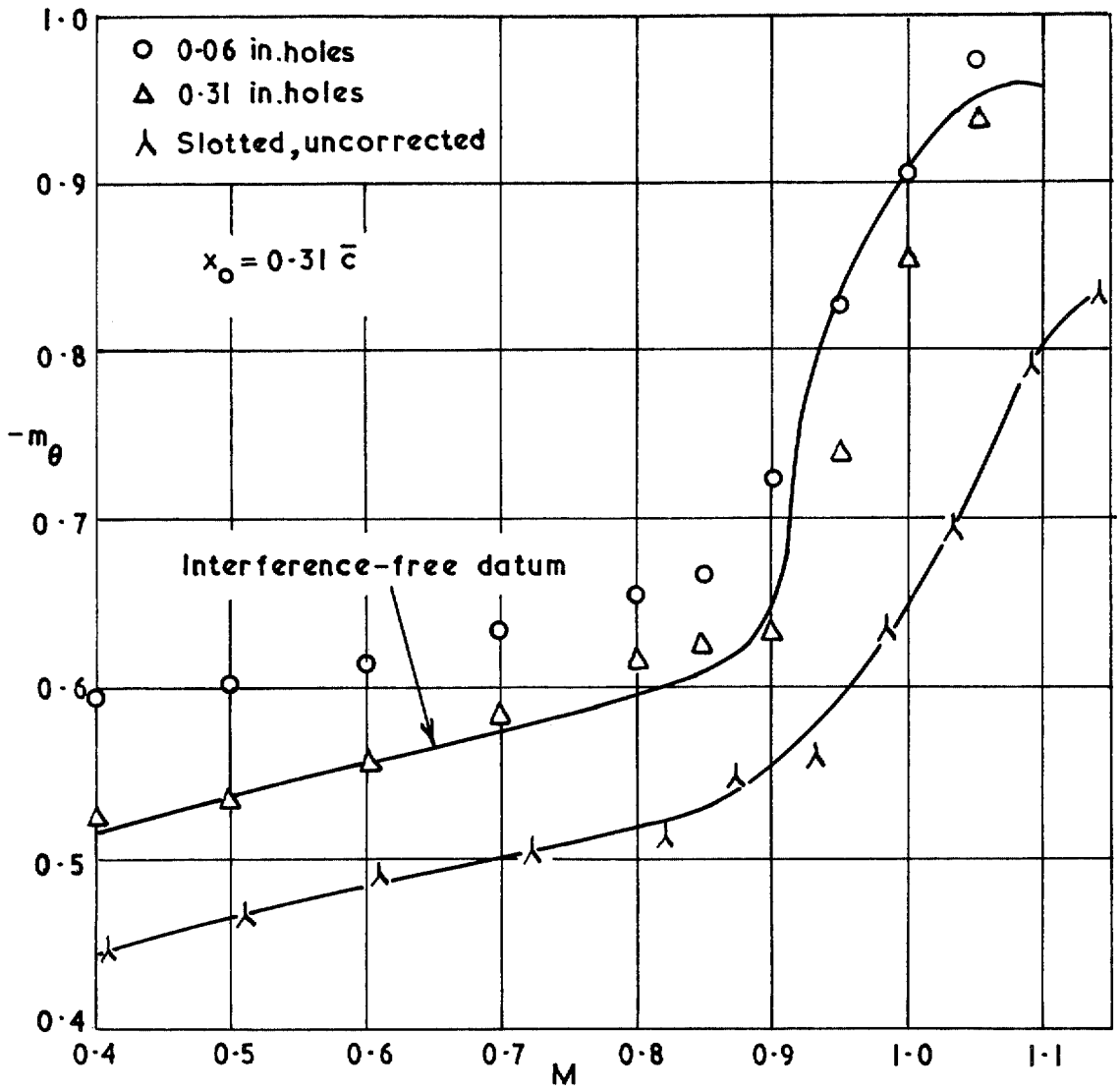


FIG. 9(c). Comparison of results from the $9\frac{1}{2}$ in × $9\frac{1}{2}$ in tunnel with interference-free values of pitching stiffness for the half-delta wing

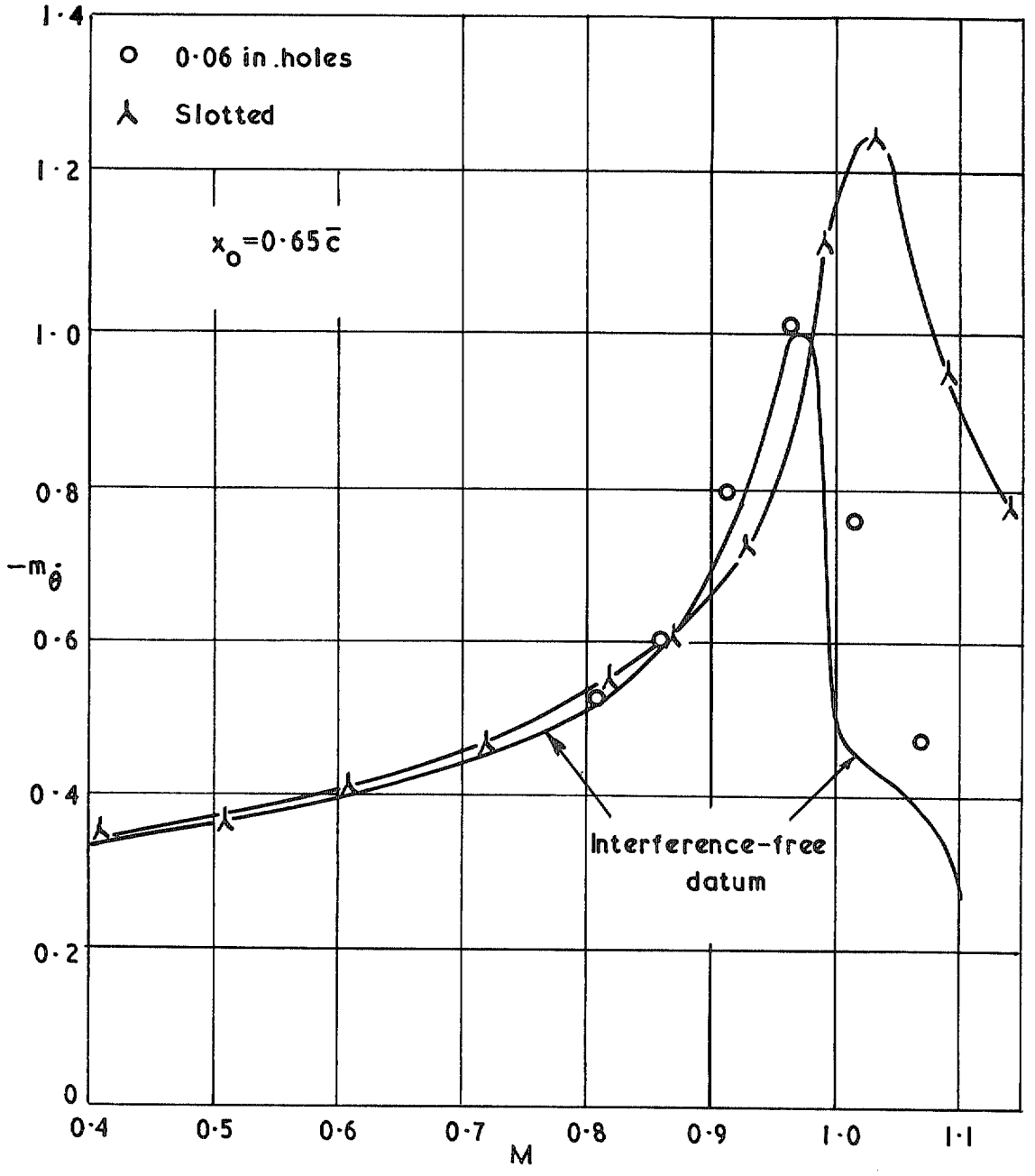


FIG. 10. Comparison of results from the $9\frac{1}{2}$ in × $9\frac{1}{2}$ in tunnel and interference-free values for the half-delta wing

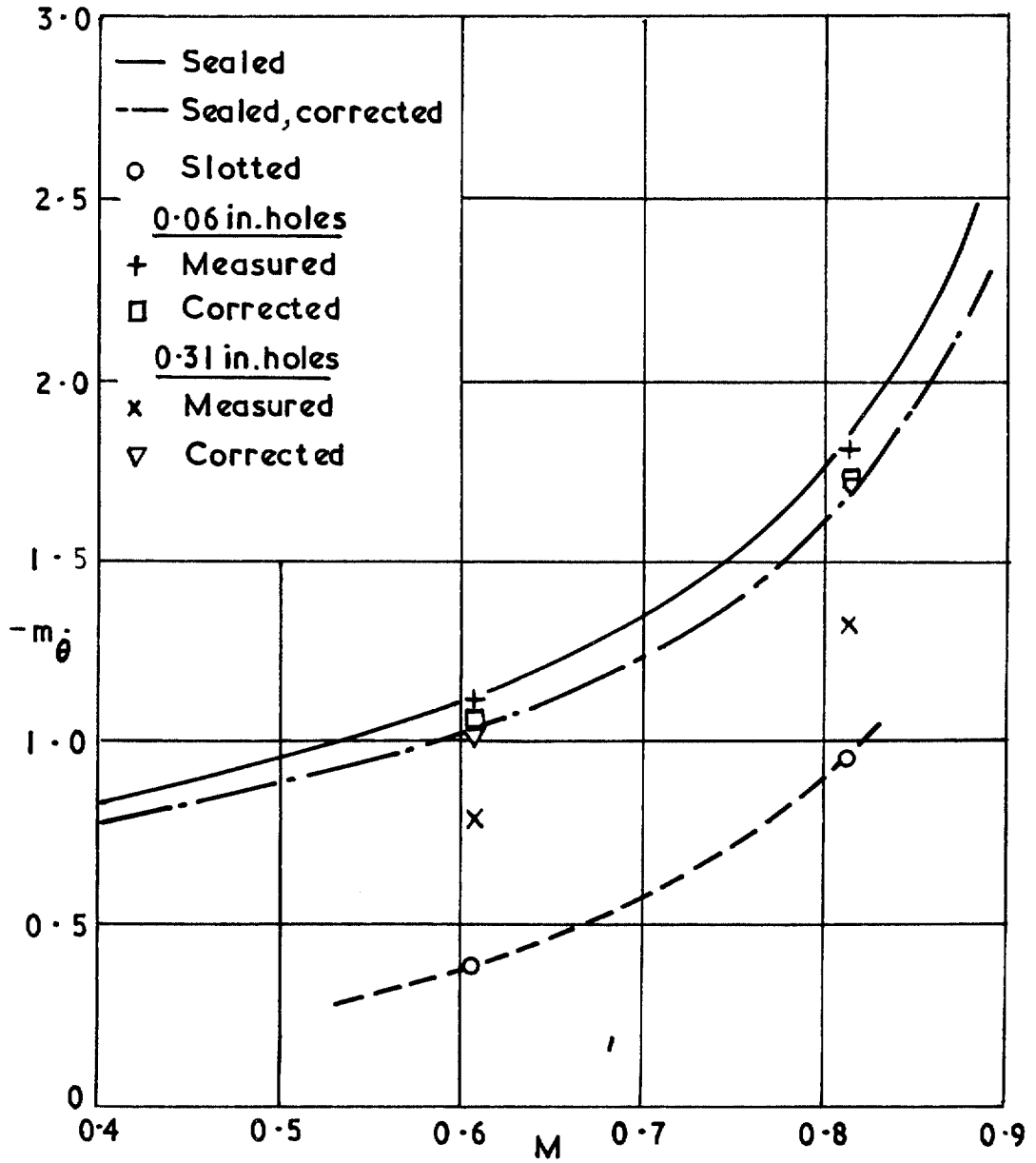


FIG. 11(a). Pitching damping for the tapered wing with various tunnel wall conditions; $x_0 = 1{\cdot}185\,\bar{c}$

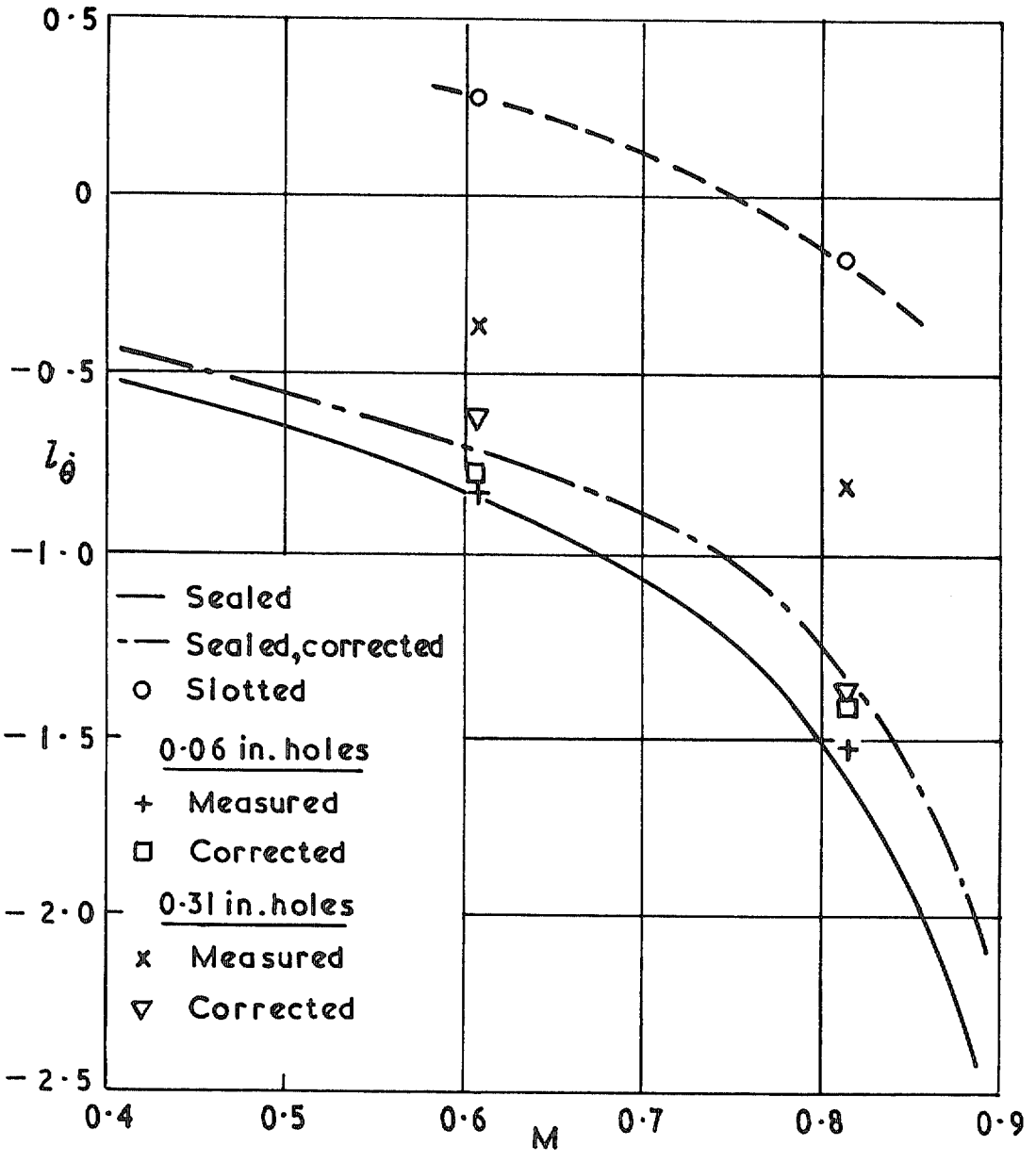


FIG. 11(b). Lift derivative $l_{\dot{\theta}}$ for the tapered wing with various tunnel wall conditions; $x_0 = 1{\cdot}185\,\bar{c}$

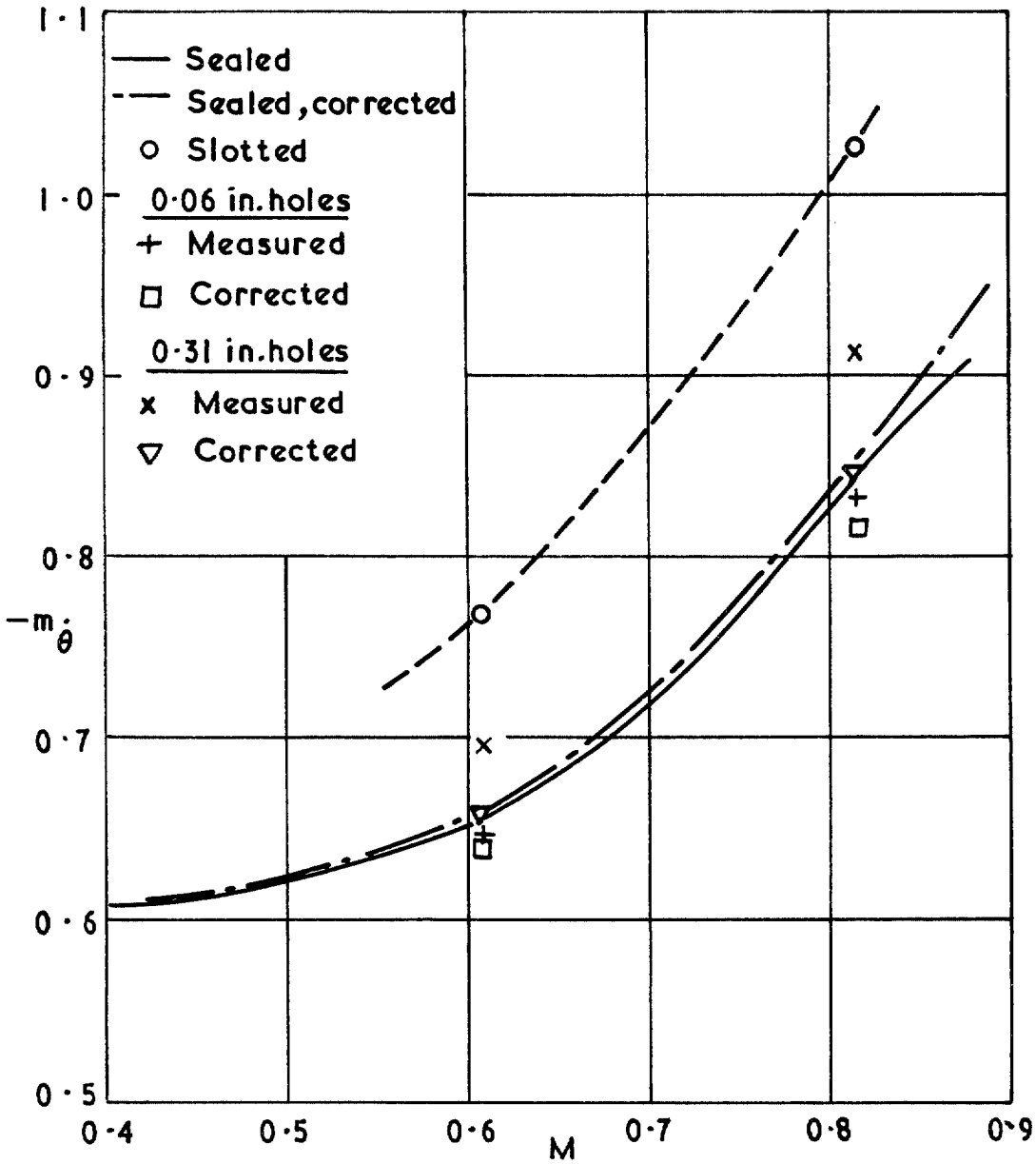


FIG. 12(a). Pitching damping for the tapered wing with various tunnel wall conditions; $x_0 = 0{\cdot}395\,\bar{c}$

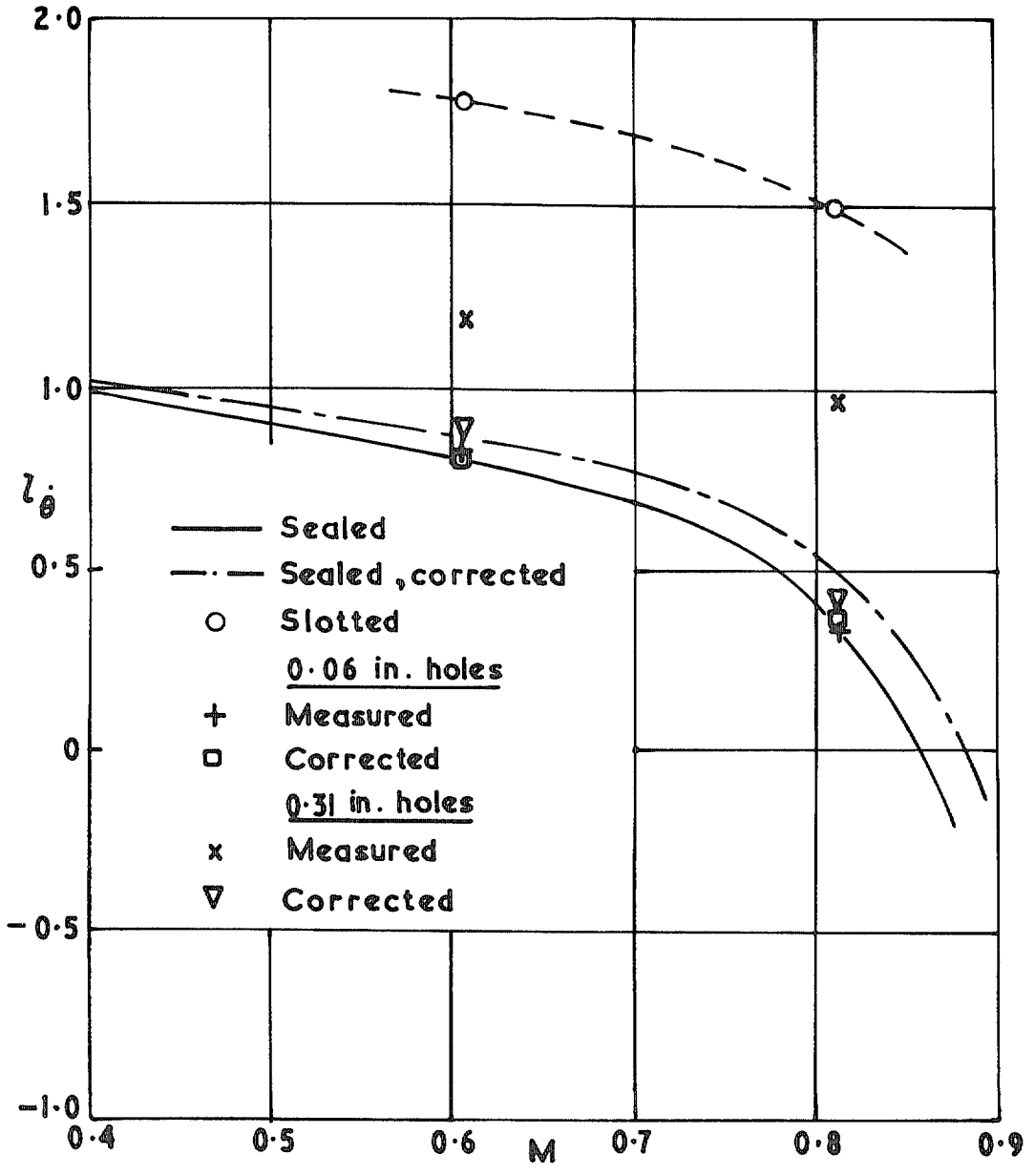


FIG. 12(b). Lift derivative $l_{\dot{\theta}}$ for the tapered wing with various tunnel wall conditions; $x_0 = 0{\cdot}395\,\bar{c}$

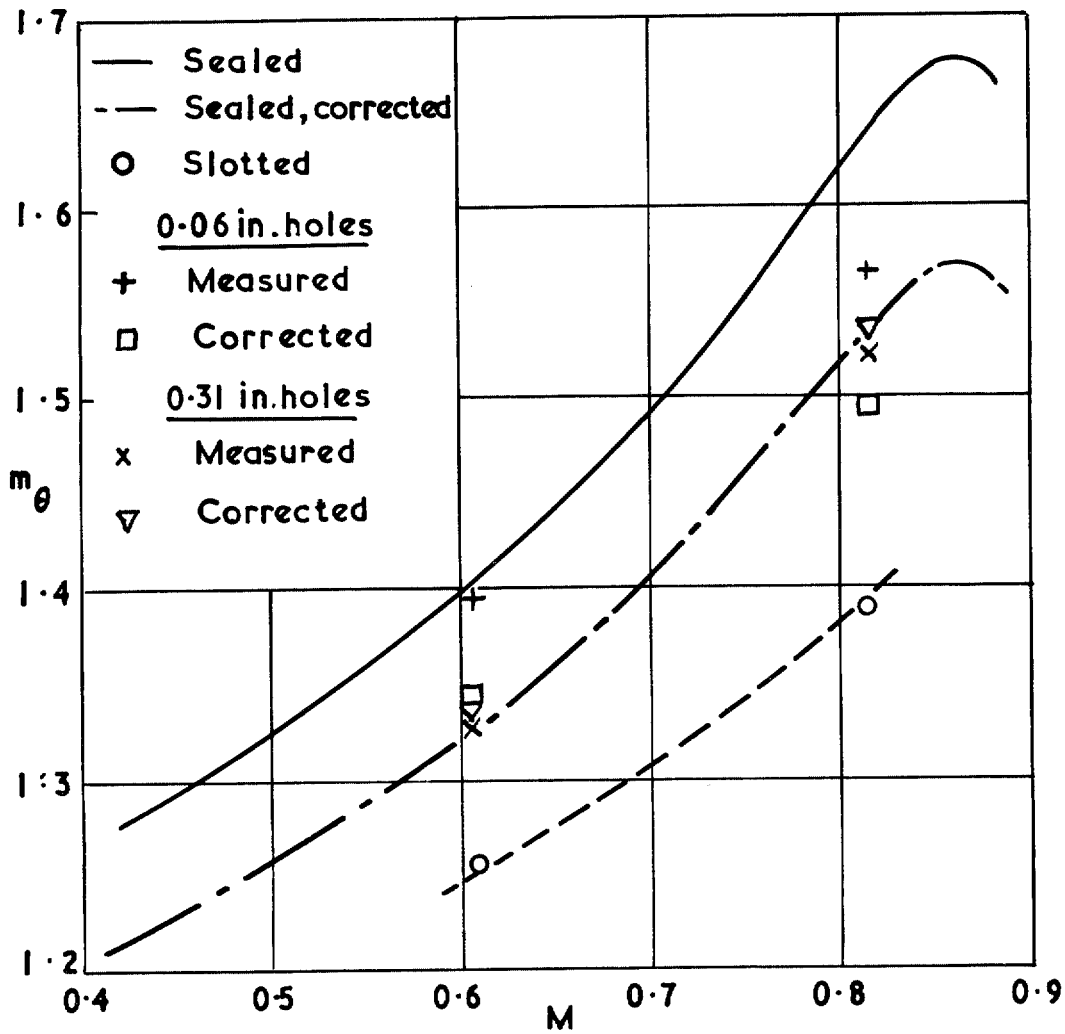


FIG. 13(a). Pitching stiffness for the tapered wing with various tunnel wall conditions; $x_0 = 1{\cdot}185\,\bar{c}$

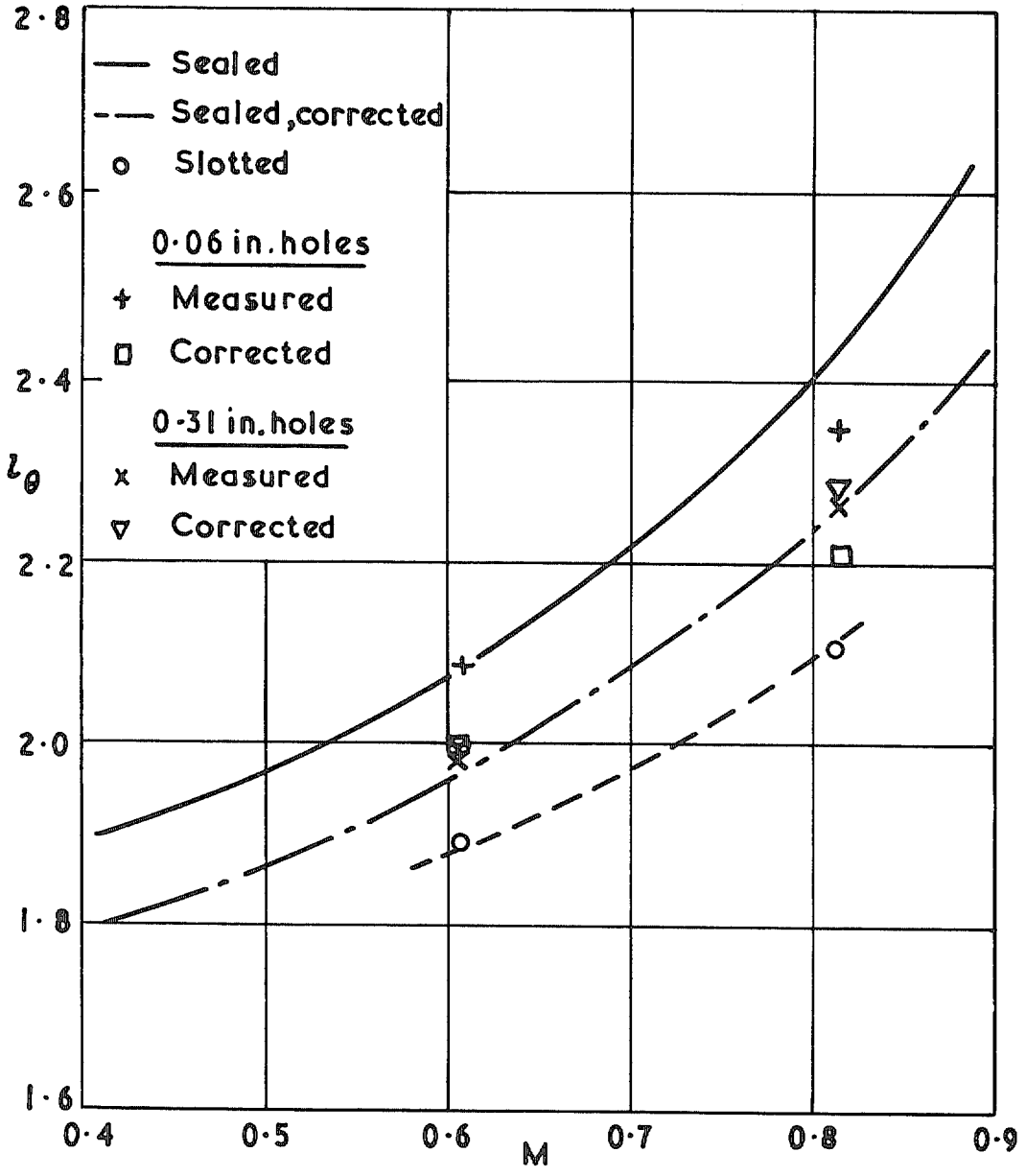


FIG. 13(b). Derivative $l_\theta$ for the tapered wing with various tunnel wall conditions

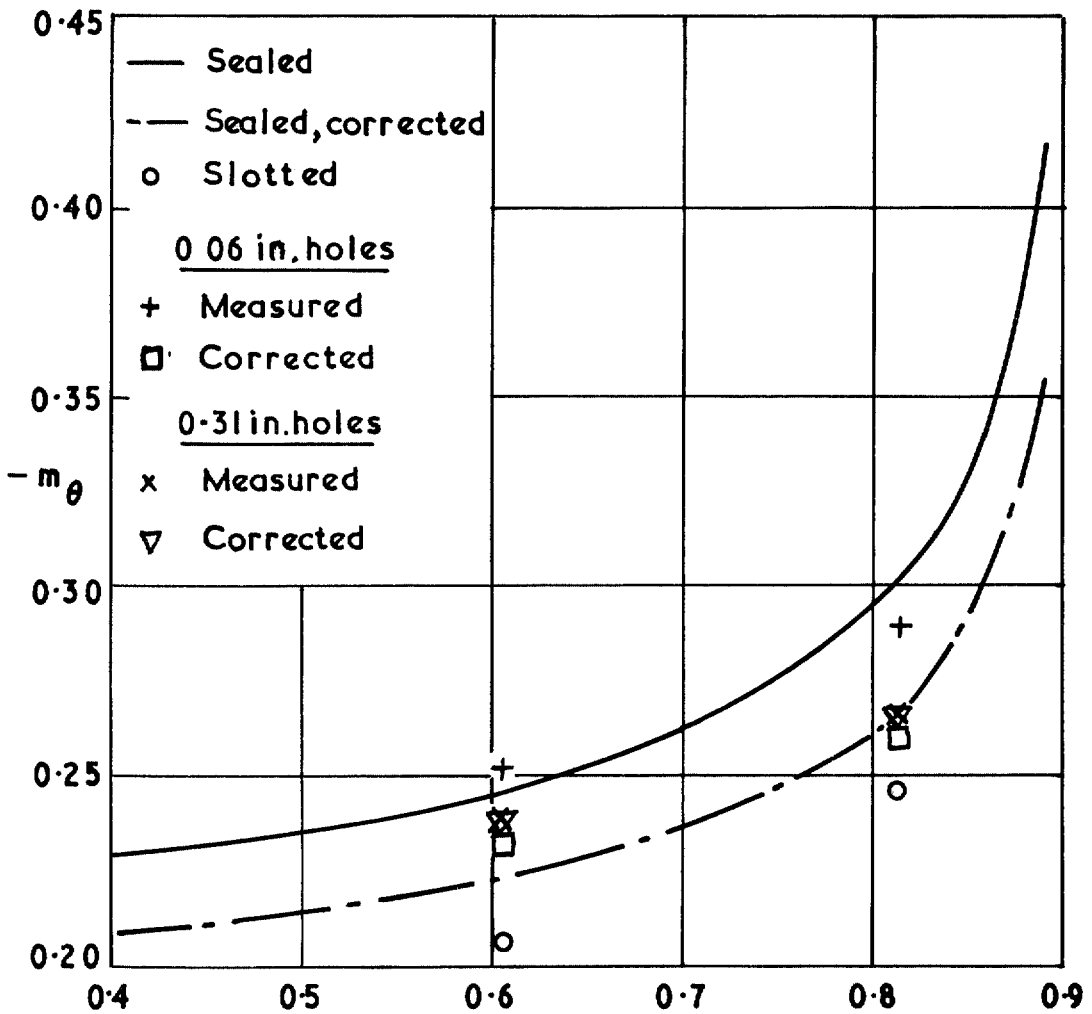


FIG. 14. Pitching stiffness for the tapered wing with various tunnel wall conditions; $x_0 = 0{\cdot}395\,\bar{c}$

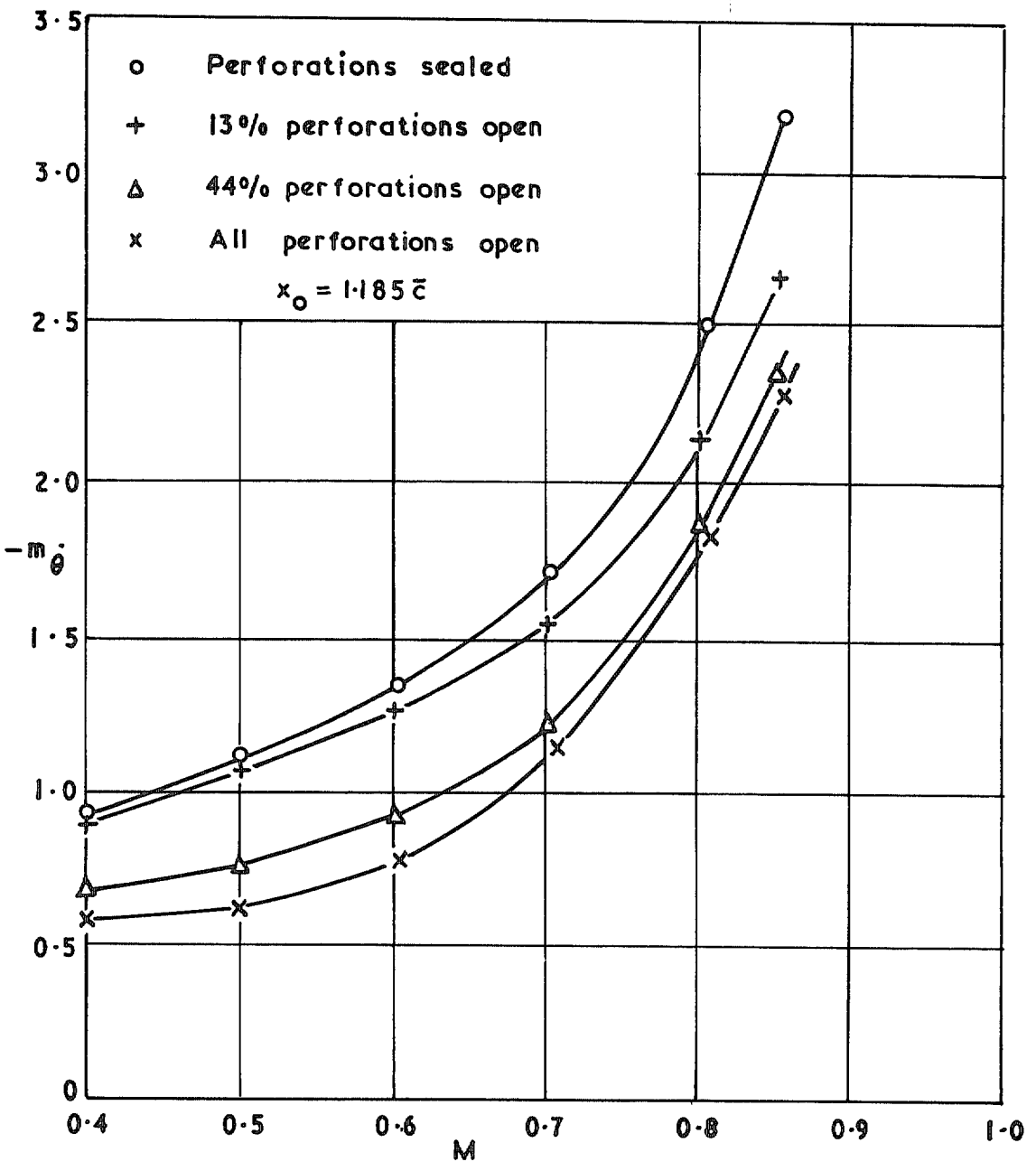


FIG. 15. Variation of $m_{\dot{\theta}}$ with M for the tapered wing of Ref. 2. in the 25 in × 20 in tunnel showing the effect of reducing the open area of the perforated walls

Printed in England for Her Majesty's Stationery Office by J. W. Arrowsmith, Bristol
Dd 503426 K5 1/73

HER MAJESTY'S STATIONERY OFFICE

*Government Bookshops*

49 High Holborn, London WC1V 6HB
13a Castle Street, Edinburgh EH2 3AR
109 St Mary Street, Cardiff CF1 1JW
Brazennose Street, Manchester M60 8AS
50 Fairfax Street, Bristol BS1 3DE
258 Broad Street, Birmingham B1 2HE
80 Chichester Street, Belfast BT1 4JY

*Government publications are also available through booksellers*


SBN 11 470515 1